



Published in final edited form as:

FASEB J. 2023 November ; 37(11): e23248. doi:10.1096/fj.202301185R.

## Identification of the novel role of sterol regulatory element binding proteins (SREBPs) in mechanotransduction and intraocular pressure regulation

Ting Wang<sup>1,2</sup>, Avinash Soundararajan<sup>1</sup>, Jeffrey Rabinowitz<sup>3</sup>, Anant Jaiswal<sup>4</sup>, Timothy Osborne<sup>4</sup>, Padmanabhan Paranjith Pattabiraman<sup>1,2,#</sup>

<sup>1</sup>Glick Eye Institute, Department of Ophthalmology, Indiana University School of Medicine, 1160 West Michigan Street, Indianapolis, Indiana, 46202, United States of America

<sup>2</sup>Stark Neuroscience Research Institute, Medical Neuroscience Graduate Program, Indiana University School of Medicine, 320 W. 15th Street, Indiana, 46202, United States of America

<sup>3</sup>Department of Ophthalmology, Case Western Reserve University, Cleveland, Ohio, United States of America

<sup>4</sup>Institute for Fundamental Biomedical Research, Department of Medicine and Biological Chemistry, Johns Hopkins University School of Medicine, St. Petersburg, Florida, 33701, United States of America

### Abstract

Trabecular meshwork (TM) cells are contractile and mechanosensitive, and they aid in maintaining intraocular pressure (IOP) homeostasis. Lipids are attributed to modulating TM contractility, with poor mechanistic understanding. In this study using human TM cells, we identify the mechanosensing role of the transcription factors sterol regulatory element binding proteins (SREBPs) involved in lipogenesis. By constitutively activating SREBPs and pharmacologically inactivating SREBPs, we have mechanistically deciphered the attributes of SREBPs in regulating the contractile properties of TM. The pharmacological inhibition of SREBPs by fatostatin and molecular inactivation of SREBPs *ex vivo* and *in vivo* respectively results in significant IOP lowering. As a proof of concept, fatostatin significantly decreased the SREBPs responsive genes and enzymes involved in lipogenic pathways as well as the levels of the phospholipid, cholesterol, and triglyceride. Further, we show that fatostatin mitigated actin polymerization machinery and stabilization, and decreased ECM synthesis and secretion. We thus postulate that lowering

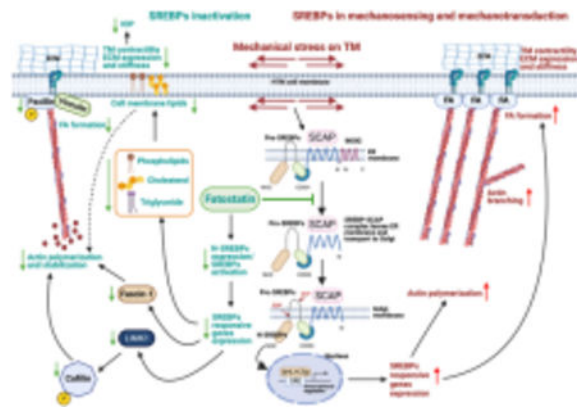
# **Corresponding Author:** Padmanabhan Pattabiraman PhD, Eugene and Marilyn Glick Eye Institute, Department of Ophthalmology, Indiana University School of Medicine, 1160 West Michigan Street, Indianapolis, IN 46202-5209, ppattabi@iu.edu, Office: 317-274-2652, Fax: 317-274-2277.

#### AUTHOR CONTRIBUTIONS

Conceptualization: Padmanabhan Paranjith Pattabiraman. Methodology, cell cultures, immunohistochemistry, immunofluorescence immunoblotting, qPCR: Ting Wang, Avinash Soundararajan, and Jeffrey Rabinowitz. Animal work—Animal Breeding & Injection: Anant Jaiswal, Ting Wang, Avinash Soundararajan, and Padmanabhan Paranjith Pattabiraman. Formal analysis: Ting Wang, Avinash Soundararajan, and Padmanabhan Paranjith Pattabiraman. Investigation: Ting Wang, Avinash Soundararajan, Jeffrey Rabinowitz, and Padmanabhan Paranjith Pattabiraman. Lipidomics data collection, data analysis, and pathway analysis: Ting Wang. Write-up and data curation: Ting Wang, Avinash Soundararajan, and Padmanabhan Paranjith Pattabiraman. Writing—original draft preparation: Ting Wang and Padmanabhan Paranjith Pattabiraman. Figure preparation: Ting Wang and Padmanabhan Paranjith Pattabiraman. Visualization: Ting Wang, Avinash Soundararajan, and Padmanabhan Paranjith Pattabiraman: supervision: Padmanabhan Paranjith Pattabiraman: project administration: Padmanabhan Paranjith Pattabiraman: funding acquisition: Padmanabhan Paranjith Pattabiraman. All authors have read and approved the manuscript.

lipogenesis in the TM outflow pathway can hold the key to lowering IOP by modifying the TM biomechanics.

## Graphical Abstract



In this study, we show the role of lipogenic transcription factors sterol regulatory element binding proteins (SREBPs) in the regulation of intraocular pressure (IOP). (**Graphical Abstract**)

- SREBPs are involved in the sensing of changes in mechanical stress on the trabecular meshwork (TM). SREBPs aid in transducing the mechanical signals to induce actin polymerization and filopodia/lamellipodia formation.
- SREBPs inactivation lowered genes and enzymes involved in lipogenesis and modified lipid levels in TM.
- SREBPs activity is a critical regulator of ECM engagement to the matrix sites.
- Inactivation of SCAP-SREBP pathway lowered IOP via actin relaxation and decreasing ECM production and deposition in TM outflow pathway signifying a novel relationship between SREBP activation status and achieving IOP homeostasis.

## Keywords

Intraocular pressure; trabecular meshwork; sterol regulatory element binding protein; mechanotransduction; lipid biogenesis; actin cytoskeleton; extracellular matrix

## 1. Introduction:

Chronic and sustained elevation in intraocular pressure (IOP) is a significant risk factor for primary open angle glaucoma (POAG) [1–3]. A rise in IOP above normal causes mechanical stress and reduced blood flow to the optic nerve [4]. This increases the risk of glaucoma with significant consequences on vision and quality of life [5–7]. Glaucoma is a major public health concern and the second leading cause of irreversible blindness worldwide afflicting mainly the aging population [8, 9]. The estimated number of glaucoma patients in the world is around 80 million with over 2 million in the United States alone [10, 11]. Interestingly lowering IOP is neuroprotective and the most effective way to delay the onset of POAG and to halt the progression towards vision loss [12–14]. A 20% decrease in IOP

significantly alleviates the risk of developing glaucoma [15]. The IOP is maintained by the balance between the generation of AH via the ciliary body and drainage mainly via the conventional outflow pathway, which includes trabecular meshwork (TM), juxtacanalicular TM tissue (JCT), and Schlemm's canal (SC) [16]. The TM contains an extracellular matrix (ECM) organized into a network of beams lined by contractile and mechanosensitive TM cells sensing pressure changes [17–22]. Increased actin contractility in TM and ECM hyperdeposition in TM outflow pathway augment AH outflow resistance and IOP elevation [23–25]. In POAG, the increased IOP is directly correlated with the increased outflow resistance, and the most characteristic structural change in TM is increased tissue stiffness including ECM accumulation, increased cell contractility, and cell-ECM connections [21, 26–28]. Thereby mitigating TM contractility and the ECM based stiffness has provided novel therapeutic options to lower IOP [29].

Cellular lipids play important roles in tissue biomechanics by modulating the plasma membrane remodeling, signal transduction cascades, and actin cytoskeleton-cell adhesions linked to the ECM [30]. Moreover, various lipids found in TM and AH are known to impact IOP homeostasis [31–33]. This is attributed via modulating the signaling events including altering the TM contractility and tissue stiffness. Hyperlipidemia is associated with an increased risk of elevated IOP and glaucoma with poor mechanistic understanding [34–36]. Interestingly, cholesterol-lowering statins lower IOP and reduce the incidence of glaucoma [37–39]. Mechanistic studies in TM point at statin-mediated disruption of membrane association of Rho GTPase due to inhibition of the isoprenylation of Rho [39, 40]. We recently found that cyclic mechanical stretch, which mimics mechanical stress on TM, significantly altered lipid contents and increased the expression of cholestogenic enzymes like squalene synthase, 3-hydroxy-3-methylglutaryl coenzyme A (HMG-CoA) synthase (HMGCS) and the transcriptional regulator of lipid biogenesis sterol regulatory element binding protein 2 (SREBP2) in human TM (HTM) cells [41]. The SREBPs are master regulator of cellular lipogenesis and occur as three isoforms – SREBP1a, SREBP1c, and SREBP2 [42–44]. SREBP1a is involved in overall lipid biosynthesis, SREBP1c regulates fatty acid synthesis, whereas SREBP2 modulates sterol biosynthesis specifically [42–45]. SREBPs are basic-helix-loop-helix leucine zipper (bHLH-LZ) transcription factors. Each SREBP precursor has three domains: (1) an NH<sub>2</sub>-terminal domain including transactivation domain, which is rich in serine and proline and the bHLH-LZ region for DNA binding and dimerization; (2) two hydrophobic transmembrane spanning segments; (3) a COOH-terminal domain [46, 47]. Within the cell, following SREBPs mRNA translation, the proform SREBPs (Pro-SREBPs) are bound to SREBP cleavage activating protein (SCAP) forming a SCAP-SREBP complex located on the ER membrane. Stimuli including low lipids levels promote SCAP to guide the whole complex to leave the ER membrane to the Golgi membrane. In the Golgi, the SCAP-SREBP complex is cleaved by site 1 protease (S1P) and site 2 protease (S2P), releasing SCAP from the complex and releasing the active or nuclear SREBPs (N-SREBPs) from Golgi to translocate into the nucleus. Inside the nucleus, N-SREBPs bind to the sterol response element (SRE) on the promoter region of the responsive genes and promote their transcription. These target genes are involved in the fatty acid, triglycerides, and cholesterol biosynthetic pathways by modulating the expression of rate limiting enzymes like acetyl-CoA carboxylase (ACC), fatty acid synthase (FAS), and

3-hydroxy-3-methylglutaryl coenzyme A (HMG-CoA) reductase (HMGCR) [45, 47–50]. Interestingly, it was earlier reported that there is an isoprenylation of RhoA-dependent and cholesterol-independent actin cytoskeleton contraction, which prevents SREBP1 dependent lipogenesis in human immortalized cancer lines and *Drosophila* [51]. Such regulatory mechanistic evaluation of lipogenic pathways in AH outflow tract and the role of SREBPs in TM biology lacks understanding. By regulating lipid biogenesis in TM, we believe that SREBPs activities play a significant role in defining actin polymerization and ECM remodeling [52–55]. Investigating the mechanosensing function via SREBPs activation paradigm in TM can elucidate how TM cells actively sense and transduce mechanical signals via SREBPs. Thus, we report the biological relevance of SREBPs activation in TM for active pressure sensing to convert mechanical stimuli into TM contractility and mechanistically decipher how the inactivation of SREBPs in the TM outflow pathway lowers IOP.

## 2. Material and Methods:

### 2.1 Materials:

The reagents and antibodies used in this study are documented in Table 1.

### 2.2 Primary TM cell culture:

Primary human TM (HTM) cells were cultured from TM tissue isolated from the leftover donor corneal rings after they had been used for corneal transplantation at the Indiana University Clinical Service, Indianapolis, and characterized as described previously [23, 56]. HIPPA compliance guidelines were adhered for the use of human tissues. The usage of donor tissues was exempt from the DHHS regulation and the IRB protocol (191117637), approved by the Indiana University School of Medicine IRB review board.

Primary porcine TM (PTM) cells were cultured from fresh porcine TM globes obtained from Indiana Packers, Delphi, IN, USA, as described previously [23].

All experiments were conducted using confluent HTM or PTM cultures as mentioned, using cells in between passage four to six, and were performed after overnight serum starvation unless mentioned, otherwise. All experiments in this manuscript were performed using biological replicates. The four HTM lines between ages 49–69 years old were used in this study have been characterized and described in our earlier publication [41].

### 2.3 Construction of replication-deficient recombinant adenovirus expressing N-SREBPs

Generation of replication-defective recombinant adenovirus expressing N-SREBPs under CMV promoter was performed using ViraPower Adenoviral Expression System (#K4930–00, Invitrogen) as described earlier [57]. N-SREBP1a (1470 bps), N-SREBP1c (1398 bps), and N-SREBP2 (1440 bps) were amplified using high-fidelity PCR (Advantage-HF 2 PCR kit, #639123; Clontech) from human pcDNA3.1–2xFLAG-SREBP1a (#26801, Addgene), pcDNA3.1–2xFLAG-SREBP1c (#26802, Addgene) and pcDNA3.1–2xFLAG-SREBP-2 (#26807, Addgene). Amplified N-SREBP1a (Ad5-N-SREBP1a), N-SREBP1c (Ad5-N-SREBP1c), and N-SREBP2 (Ad5-N-SREBP2) were purified, and titers determined.

## 2.4 Adenovirus-mediated gene transduction in HTM cells

Primary HTM cells were grown on gelatin-coated glass coverslips or in plastic Petri dishes and were infected with Ad5-N-SREBP1a, Ad5-N-SREBP1c, and Ad5-N-SREBP2 or a control empty virus (AdMT) at 50 multiplicities of infection for 24 h followed by 48 h serum starvation. Cells were then washed with 1X PBS and were fixed for immunofluorescence (IF) analysis and collected using either TRIZOL for RNA extraction or 1X radioimmunoprecipitation assay (RIPA) for protein extraction.

## 2.5 Optimization fatostatin for *in vitro* dosing

Fatostatin directly binds to SCAP and inhibits the SREBP-escorting function of SCAP, thereby restricting the translocation of SREBPs from ER to the Golgi and subsequently causing SREBPs inactivation and reducing lipogenesis and fat accumulation [58–60]. Overnight serum starvation (~16 h) was carried out on PTM and HTM cultures before treatments. To identify the optimal concentration of fatostatin for lowering SREBPs activation, PTM cells were subjected to 0.2, 2, and 20  $\mu\text{M}$  fatostatin in dimethyl sulfoxide (DMSO) reconstituted in serum-free DMEM for 24 h, respectively, and the solvent DMSO treated PTM cells were used as a control. Post-treatment, PTM cells were either used for cell viability assay or protein collected for total and nuclear fraction. HTM cells were subjected to the optimal concentration of fatostatin and post-treatment, cells were collected in TRIZOL for RNA isolation or in 1X radioimmunoprecipitation assay (RIPA) buffer for protein isolation along with the cell culture media and stored in  $-80^{\circ}\text{C}$  until used.

## 2.6 Cell viability assay

The cell viability assay was performed using fluorescein diacetate (FDA) and propidium iodide (PI) staining. PTM cells were grown in 6-well plates until they attained 90% confluency. The cells were treated with a final concentration of 20  $\mu\text{M}$  fatostatin for 24 h after overnight serum starvation. FDA-PI double staining was performed based on a previously published protocol with minor modifications [61].

## 2.7 Cyclic mechanical Stretch:

HTM cells were plated on BioFlex<sup>®</sup> Culture Plates (Flexcell International Corp) and subjected to cyclic mechanical stretch as published earlier [41]. The cells were subjected to cyclic mechanical stretch at 0.69 Hz frequency with 15% stretching. 2 h and 6 h post stretch, cells were fixed and processed for IF analysis.

## 2.8 *Ex vivo* porcine anterior segment elevated IOP model

Elevated IOP was modeled using porcine *ex vivo* perfusion system as described earlier [23, 57]. Post perfusion the TM tissue was carefully isolated and frozen at  $-80^{\circ}\text{C}$  until further processing.

## 2.9 *Ex vivo* porcine anterior segment perfusion culture to assess the effect of SREBPs inactivation on IOP

The effect of pharmacological SREBPs inactivation on IOP regulation was studied using *ex vivo* porcine anterior segment perfusion culture as described earlier [23]. After achieving

a stable baseline IOP, the IOP was continuously recorded in the control eyes that received a sham DMSO treatment, and the experimental eyes received 20  $\mu$ M fatostatin for up to 24h. The relative changes in IOP were calculated as the change in pressure relative to the baseline of drug/sham perfusion. At the end of the perfusion studies, TM tissues were either sectioned for histology studies and fixed with 4% paraformaldehyde, or the TM was collected for protein analysis.

## 2.10 SCAP-Floxed (*SCAP<sup>fl/fl</sup>*) mice

All experiments were performed in compliance with the Association for Research in Vision and Ophthalmology (ARVO) Statement for the Use of Animals in Ophthalmic and Vision Research. Mice carrying the floxed Scap allele (B6;129-*Scap<sup>tm1Mbjg/J</sup>*) [48] were obtained from Dr. Tim Osborne, bred, and housed under a standard 12 h light and dark cycle with food and water provided *ad libitum* in the laboratory animal resource center (LARC). Exon 1 of the SCAP gene is flanked with LoxP sites, which are targets for bacteriophage P1 Cre recombinase originally made by Dr. Horton, UTSW Med Center, Dallas [48, 62]. They are viable, fertile, normal in size, and do not display any physical or behavioral abnormalities. The genotype was identified by PCR analysis of tail biopsies. All animal procedures were approved by the Institutional Animal Care and Use Committee at the Indiana University School of Medicine and conducted following the Declaration of Helsinki.

## 2.11 Molecular inactivation of SREBPs *in vivo* in *SCAP<sup>fl/fl</sup>* mice

Molecular inactivation of SREBPs was achieved by knocking down SCAP in *SCAP<sup>fl/fl</sup>* mice via intravitreal injection of adenovirus expressing Cre [Ad5.CMV.iCre-eGFP] ( $1.6 \times 10^{11}$  pfu/ml). The Ad5.CMV.eGFP ( $2.6 \times 10^{11}$  pfu/ml) was used as an adenovirus control and saline injection was used for injection control. These adenoviruses were purchased from the Vector Development Lab, Baylor College of Medicine. Four groups were included in the study: untouched, saline injection, Ad5.CMV.eGFP injection, and Ad5.CMV.Cre-eGFP injection. A 33-gauge needle with a glass microsyringe (10  $\mu$ L volume; Hamilton Company) was used for the intravitreal injection. Intravitreal injections were performed only in the left eye under a surgical microscope (Trinocular Stereo Zoom Microscope, AmScope). The needle was inserted through the equatorial sclera into the vitreous chamber at an angle of  $\sim 45^\circ$ , carefully avoiding contact with the posterior lens capsule or the retina. The right eyes in all groups were left untouched. Viral vectors or saline in a volume of 2  $\mu$ L were slowly injected into the vitreous over the course of 30 seconds. The final concentration was  $3.2 \times 10^8$  pfu for Ad5.CMV.iCre-eGFP and  $5.2 \times 10^8$  pfu for Ad5.CMV.eGFP. The needle was then left in place for an additional 45 s to avoid leakage before being withdrawn. Before and during intravitreal injection, mice were anesthetized with isoflurane (2.5%) (#NDC 46066-755-04, Patterson Veterinary, Loveland, CO, USA) and 100% oxygen using SomnoSuite (Kent Scientific Corporation, Torrington, CT, USA). Initially, a total of 15 animals/group were used, but post-injection due to infection, cataract formation, and death the final numbers were reduced to 9–10 mice/group for the data acquisition with a roughly equal number of adult (10–14 months) and old (18–24 months) mice.

## 2.12 Measurement of IOP

The mice were anesthetized with 2.5% isoflurane and 100% oxygen using SomnoSuite. A previously validated commercial rebound tonometer (TonoLab, Colonial Medical Supply) was used to take three sets of six measurements of IOP in each eye. The IOP measurement and recording were carried out in a blinded manner by the experimenter to minimize outcome bias. Right and left eye measurement sets were alternated with the initial eye selected randomly. All measurements were taken between 3 and 5 min after isoflurane inhalation. As indicated by the manufacturer, the tonometer was fixed horizontally for all measurements, and the tip of the probe was 2–3 mm from the eye. The probe contacted the eye perpendicularly over the central cornea. The average of a set of measurements was accepted only if the device indicated that there was “no significant variability” (as per the protocol manual; Colonial Medical Supply). Daytime measurements were taken between 10:00 and 15:00 h. Baseline IOP was measured before saline and viral vector injection. After injection, IOP was measured every 10 days until 50 days post-injection.

## 2.13 Gene expression analysis

Total RNA was extracted from HTM cells using the Trizol method following the manufacturer’s protocol. The RNA amount used, cDNA conversion, and using reverse-transcription polymerase chain reaction (RT-PCR), and qPCR reaction were conducted as published before [57]. Sequence-specific forward and reverse oligonucleotide primers for the indicated genes are provided in Table 2. The qPCR reaction was performed and calculated by the delta-delta Ct method as described earlier [57, 63]. The normalization was performed using 18S ribosomal RNA (18S rRNA) for HTM.

## 2.14 Protein Analysis by Immunoblotting

For nuclear fraction, cells were collected from a 10 cm plate using fractionation buffer (20 mM HEPES, 10 mM KCl, 2 mM MgCl<sub>2</sub>, 1 mM EDTA, 1 mM EGTA, 1 mM DTT). After using a 1 mL syringe to pass cell suspension through a 27 gauge needle several times, the sample was centrifuged and a pellet that contains nuclei was collected. The pellet was washed, dispersed, and centrifuged again, then the nuclear fraction was collected by TBS with 0.1% SDS.

The whole cell lysates containing total protein were prepared using 1X RIPA buffer composed of 50 mM Tris-HCL (pH 7.2), 150 mM NaCl, 1% NP-40, 0.1% SDS, 1 mM EDTA, and 1 mM PMSF with protease and phosphatase inhibitors (#A32961, ThermoFisher Scientific) and then sonicated. Nuclear extraction was collected using 20mM HEPES (pH 7.4), 10mM KCl, 2mM MgCl<sub>2</sub>, 1mM EDTA, and 1mM EGTA. Media was collected, concentrated using Nanosep<sup>®</sup> Centrifugal Devices with Omega<sup>™</sup> Membrane 10K (#OD010C34, Pall), and the media protein was collected in 1X RIPA.

After determining the protein concentration, immunoblotting was performed as published earlier [41, 57]. Blots were stripped using mild stripping buffer if required to reprobe for the loading control and multiple proteins within the same molecular weight range. The data were normalized to GAPDH,  $\beta$ -actin, LaminB1, or Ponceau S. Semi-quantitative analyses and fold changes were calculated from the band intensities measured using ImageJ software.

### 2.15 Protein distribution analysis by immunohistochemistry (IHC) and IF

Tissue sections from formalin-fixed, paraffin-embedded human donor whole globes eyes were prepared at Case Western Reserve University, Cleveland, Ohio. Paraffin-embedded porcine TM tissue slides and mice eyeball slides were prepared at the Histology Core, Indiana University, and immunolabeling was performed. IF staining was done on HTM cells grown on 2% gelatin-coated glass coverslip or BioFlex® Culture Plates. The methodologies used for IHC and IF has been published from the lab earlier [23, 57].

All the slides were observed under a Zeiss LSM 700 confocal microscope, and z-stack images were obtained and processed using Zeiss ZEN image analysis software.

### 2.16 Quantitative image analysis

ImageJ (version 1.53a) software was used to analyze the SREBPs nuclear fluorescence intensity in IF HTM cell images and ECM proteins in IHC tissue images. Specifically, the IF images obtained from HTM cells and tissue sections were converted into an 8-bit image, then the threshold default setup under Adjust was used to convert the image from grayscale into a binary image. Next, the region of interest (ROI) tool was utilized for analysis. In this analysis, the nuclear area in the HTM cells or ROIs (equal area) in the TM outflow pathway was chosen in an image, and the intensities were measured and compared between the DMSO control and fatostatin.

### 2.17 Quantitative filamentous actin/globular actin (F-actin/G-actin) ratio measurement

The F-actin/G-actin ratio was measured using G-Actin/F-Actin In Vivo Assay Biochem Kit (#BK037, Cytoskeleton, Inc.), following the manufacturer's instructions.

### 2.18 Myosin light-chain (MLC) phosphorylation status measurement

The phosphorylation status of MLC in HTM cells was measured by following the procedure described earlier [64]. Specifically, after treatments, HTM cells were incubated with 10% cold trichloroacetic acid (TCA) for 5 minutes and then washed with ice-cold water 5 times to completely remove the TCA. The cells were extracted with 8 M urea buffer containing 20 mM Tris, 23 mM glycine, 10 mM dithiothreitol (DTT), saturated sucrose, and 0.004% bromophenol, using a sonicator. The urea-solubilized samples were separated on urea/glycerol PAGE containing 30% acrylamide, 1.5% bisacrylamide, 40% glycerol, 20 mM Tris, and 23 mM glycine. Then proteins from these glycerol gels were transferred onto nitrocellulose filters in 10 mM sodium phosphate buffer, pH 7.6. Membranes were probed using phospho-myosin light chain (p-MLC) or myosin light chain (MLC) primary antibodies.

### 2.19 Lipid content measurement

HTM cells were plated on 100 mm plates. Post-treatment, cells were counted, equal numbers were collected, and frozen at  $-80^{\circ}\text{C}$  until analysis. Then the phospholipid, cholesterol, and triglyceride from HTM cells were extracted and measured with a phospholipid quantification assay kit (#CS0001, Sigma-Aldrich), cholesterol quantitation kit



(#MAK043, Sigma-Aldrich) and triglyceride quantification kit (#MAK266, Sigma-Aldrich) respectively, following manufacturer's instructions.

## 2.20 Cellular lipid extraction and multiple reaction monitoring (MRM) profiling-based MS for lipidomics and pathway analysis

HTM cell pellets were collected from DMSO and fatostatin treated HTM cells. The lipid extraction was performed as per the Bligh and Dyer protocol [65]. Lipidomics and data analysis were processed as published earlier [41, 66]. In addition, pathway enrichment analysis was also performed to identify the most relevant pathways associated with the identified metabolites using a web-based analysis module (<http://metaboanalyst.ca>), which is based on Globaltest. Through pathway analysis, 8 metabolic pathways related to the identified metabolites (n = 274) were mapped.

## 2.21 Transmission electron microscope (TEM) imaging

HTM cells grown on coverslips were treated with Ad5-N-SREBP1a, Ad5-N-SREBP1c, Ad5-N-SREBP2 or AdMT for 48–72 h. After removing the growth media from each well, the coverslips were washed using 0.1 M Cacodylate buffer and submerged in 3% glutaraldehyde solution and 2% OsO<sub>4</sub> subsequently. Then the cells were dehydrated by 30%, 50%, 70%, 95%, and 100% EtOH consequently, and 1:3 acetone:EMbed 812 was applied overnight. The next day, the coverslips were embedded using EMbed 812 resin in a BEEM capsule for 24 hours. After that, the samples were detached from coverslips using liquid nitrogen and then sectioned using a razor blade to generate EM grids for imaging. The grids were stained with 4% uranyl acetate and 0.2% aqueous lead citrate and washed, then imaged on a PEI Tecnai 12 with a LaB<sub>6</sub> crystal at 120kV at the Center for Electron Microscopy, IUSM.

## 2.22 Statistical analysis

All data presented were based on greater than three independent observations and inclusion of biological replicates for *in vitro* analysis. The graphs represent the mean  $\pm$  standard error. All statistical analyses were performed using Prism 9.3.1 (GraphPad). The difference between the two groups was assessed using paired Student's t-test when parametric statistical testing was applicable. When multiple groups were compared, a two-way analysis of variance followed by the Tukey post hoc test was applied. The p-value < 0.05 was considered a statistically significant difference between the test and control.

## 2.23 Ethics approval

Ethical review and approval were waived for the use of cadaveric human eyes for the isolation of the TM cells from human cadaveric corneal rims for this study. The animal study was reviewed and approved for all the procedures by the Institutional Animal Care and Use Committee at Indiana University School of Medicine under the Protocol number 19152.

### 3. Results:

#### 3.1 SREBPs and SCAP are expressed in the human AH outflow pathway and TM cell cultures

Initially we checked for the expression and distribution of SREBPs and SCAP in human TM outflow pathway (Supplementary Fig. 1) since it has never been investigated earlier. We found the expression of SREBP isoforms and SCAP transcripts in HTM cells in primary HTM cell cultures (Supplementary Fig. 1a). Additionally, the SREBP isoforms and SCAP protein were found in HTM and PTM cells. We observed pro-SREBP1 and pro-SREBP2 at ~ 125 kDa, N-SREBP1 and N-SREBP2 at ~ 68 kDa, and SCAP at ~ 140 kDa (Supplementary Fig. 1b and 1c). IF analysis and confocal imaging of SREBP1, 2, and SCAP distribution in HTM cells and the conventional human AH outflow pathway show their distinct localizations. In HTM cells, both SREBP1 and 2 showed cytoplasmic and nuclear distribution (Supplementary Fig. 1d). Relatively, SREBP1 decorated the cytoplasmic and perinuclear region around the ER than in the nucleus. On the other hand, SREBP2 showed a pronounced nuclear localization than cytoplasmic. The SCAP showed cytoplasmic distribution (Supplementary Fig. 1d). In the anterior chamber angle of a normal human eye, the SREBP1, SREBP2, and SCAP immunopositive cells were seen in the TM-JCT region and the endothelial lining of the SC (Supplementary Fig. 1e). Interestingly, SREBP1 and 2, as well as SCAP showed specific distribution in the TM-JCT region in the anterior chamber angle. Negative control in the presence of secondary antibody alone did not show any staining (Supplementary Fig. 1f).

#### 3.2 Mechanosensing via SREBPs activation in HTM cells aids in increasing the actin-based contractile changes and lamellipodia formation

In our recent work [41] on HTM cells subjected to mechanical stress, we showed a significant increase in the N-SREBP2 that is involved in cholesterol biogenesis. To better understand the mechanosensing functionality of SREBPs, here we provide empirical evidence by utilizing multiple systems to assess the potential changes qualitatively and quantitatively in SREBPs localization under mechanical stress. Firstly, we performed IF analysis post cyclic mechanical stretch to look at the changes in the localization of SREBPs (in green) and F-actin (in red) changes in a time-dependent manner at 2 h and 6 h. After 2 h of stretch (ST), HTM cells showed strong nuclear localization of SREBP1 (Fig. 1a, second-row third column) and SREBP2 (Fig. 1b, second-row third column), compared to 2 h unstretched control (CTL) (Fig. 1a and 1b, first-row third column). HTM cells also showed increased F-actin fibers formation (Fig. 1a and 1b, second-row fourth column) after 2 h ST, compared to the 2 h CTL (Fig. 1a and 1b, first-row fourth column). Image analysis using ImageJ found significantly increased fluorescent intensity for nuclear SREBP1 ( $n = 30-40$ ,  $p = 0.002$ ) and SREBP2 ( $n = 30-40$ ,  $p = 0.0001$ ) in HTM cells after 2 h ST, compared to 2 h CTL (Fig. 1a and 1b, right panel). Further we found that such increased nuclear SREBPs paralleled with increased F-actin formation in stretched HTM cells. HTM cells were exposed to 2 h ST combined with the pharmacological inhibition of SREBPs activity using fatostatin treatment, a specific SREBPs inhibitor. To test the inhibitory effect of fatostatin on SREBPs activity in TM, the dose-dependency (0.2, 2, 20  $\mu\text{M}$ ) of fatostatin on PTM cells was performed. We found that 20  $\mu\text{M}$  fatostatin for 24 h treatment significantly

decreased both N-SREBP1 ( $n = 4$ ,  $p = 0.02$ ) and N-SREBP2 ( $n = 4$ ,  $p = 0.02$ ) from the total protein extract (Supplementary Fig. 2a and 2b). The 20  $\mu\text{M}$  fatostatin did not show cytotoxic effects when tested using FDA and PI staining (Supplementary Fig. 2c). Thus, 20  $\mu\text{M}$  fatostatin is the optimal concentration to be used in TM cells. IF shows that compared to 2 h ST alone, 2 h ST combined with 20  $\mu\text{M}$  fatostatin treatment reduced both SREBP1 (Fig. 1a, third-row third column) and SREBP2 (Fig. 1b, third-row third column) localization inside the nucleus, and a concomitant decrease in F-actin distribution inside the HTM cells (Fig. 1a and 1b, third-row fourth column). Image analysis found that compared to 2 h ST alone, 2 h ST in combination with fatostatin significantly decreased nuclear SREBP1 ( $n = 30\text{--}40$ ,  $p = 0.0001$ ) and SREBP2 ( $n = 30\text{--}40$ ,  $p = 0.0001$ ) fluorescent intensity in HTM cells. Compared to 2 h CTL, 2 h ST combined with 20  $\mu\text{M}$  fatostatin treatment significantly decreased nuclear SREBP1 fluorescent intensity ( $n = 30\text{--}40$ ,  $p = 0.0001$ ), but nuclear SREBP2 didn't show significant changes ( $n = 30\text{--}40$ ,  $p = 0.2$ ) (Fig. 1a and 1b, right panel). Similar results were found after 6 h ST in HTM cells with strong nuclear localization of SREBP1 (Supplementary Fig. 3a, second-row third column) and SREBP2 (Supplementary Fig. 3b, second-row third column), and increased F-actin formation (Supplementary Fig. 3a and 3b, second-row fourth column) compared to 6 h CTL (Supplementary Fig. 3a and 3b, first-row third and fourth column, respectively). Image analysis comparing 6 h CTL versus 6 h ST showed significant increase in nuclear SREBP1 ( $n = 30\text{--}40$ ,  $p = 0.0001$ ) and SREBP2 ( $n = 30\text{--}40$ ,  $p = 0.0001$ ) fluorescent intensity in HTM cells (Supplementary Fig. 3a and 3b, right panel). 'n' here refers to the use of HTM cells as biological replicates of 2 cell strains with experimental replicates of 2. Additional evidence for the role of SREBPs in mechanosensing was obtained using the acute anterior chamber pressure model [23, 57, 67]. Porcine anterior segments when subjected to two times (2x) elevated pressure (30 mmHg) compared to normal pressure (15 mmHg), we found a significant increase in N-SREBP1 ( $n = 4$ ,  $p = 0.04$ ) and N-SREBP2 ( $n = 4$ ,  $p = 0.03$ ) (Fig. 1c). 'n' here refers to the use of HTM cells as biological replicates of 4 cell strains. Thus, confirming that novel role of SREBPs activation as the hallmark of mechanosensing in TM.

Since we found that augmented SREBPs activation paralleled with increased actin polymerization under mechanical stress in HTM cells, we assessed if SREBPs activation aided in mechanotransduction. To study this, we expressed Ad5-N-SREBPs in primary HTM cells *in vitro* and followed up with read outs including cell shape changes, actin polymerization, and focal adhesion distribution changes. In serum-starved HTM cells upon constitutively expression Ad5-N-SREBPs, Ad5-N-SREBP1a and Ad5-N-SREBP1c significantly increased N-SREBP1 transcripts ( $n = 4$ ,  $p = 0.01$  and  $n = 4$ ,  $p = 0.046$ , respectively), Ad5-N-SREBP2 significantly increased N-SREBP2 mRNA expression ( $n = 4$ ,  $p = 0.01$ ) (Supplementary Fig. 4a) in comparison to AdMT control. Similarly, N-SREBP1 protein expression significantly increased under Ad5-N-SREBP1a ( $n = 4$ ,  $p = 0.0001$ ) and Ad5-N-SREBP1c ( $n = 4$ ,  $p = 0.03$ ) and N-SREBP2 significantly increased under Ad5-N-SREBP2 ( $n = 4$ ,  $p = 0.0005$ ) (Supplementary Fig. 4b). 'n' here refers to the use of HTM cells as biological replicates of 4 cell strains. Upon examination under light microscopy, the HTM cells treated with Ad5-N-SREBPs showed altered cell shape with qualitative changes in lamellipodia and filopodial extensions (Supplementary Fig. 4c, denoted by black arrows). The increase in N-SREBPs distribution (red staining) inside the nucleus were confirmed

by IF imaging studies. A strong nuclear localization of SREBP1 was observed under Ad5-N-SREBP1a (Fig. 2a) (second-row third column) and Ad5-N-SREBP1c (third-row third column) compared to AdMT (first-row third column) and SREBP2 distribution inside the nucleus (Fig. 2b) due to Ad5-N-SREBP2 (second-row third column) compared with AdMT (first-row third column). In comparison to AdMT (Fig. 2a and 2b, first-row fifth column), Ad5-N-SREBP1a (Fig. 2a, second-row fifth column), Ad5-N-SREBP1c (Fig. 2a, third-row fifth column), and Ad5-N-SREBP2 (Fig. 2b, second-row fifth column) expression increased F-actin distribution inside HTM cells (purple staining in the merged/individually in grayscale) indicating greater actin polymerization. This was accompanied by redistribution of the focal adhesions - vinculin (in green) in the merged/individually in grayscale (denoted by white arrows) at the edges of F-actin was observed in Ad5-N-SREBP1a (Fig. 2a, second-row fourth column), Ad5-N-SREBP1c (Fig. 2a, third-row fourth column), and Ad5-N-SREBP2 (Fig. 2b, second-row fourth column). An interesting observation we found was a qualitative increase in lamellipodia and filopodia formation with a strong lamellipodial actin network (Fig. 2a and 2b, denoted by yellow arrows). Similar observations were found for paxillin distribution in TM cells under constitutive activation of SREBPs (Supplementary Fig. 4d and 4e). Further investigations into the lamellipodial structures identified strong localization of actin binding protein Arp2/3, which is involved in branching of fibrillar actin, and the regulator of lamellipodial dynamics Ras-associated and pleckstrin homology domains-containing protein 1 (RAPH1) or lamellipodin (in green) to membrane under constitutive activation of SREBP1a, 1c, and 2 (Fig. 2c, denoted by white arrows). The ultrastructural examination of constitutive SREBPs activation using TEM showed that compared to AdMT treatment, Ad5-N-SREBP1a, Ad5-N-SREBP1c and Ad5-N-SREBP2 treatments induced membrane bending and filopodia formation in HTM cells (Fig. 2d) corroborating with results from IF. Interestingly, all Ad5-N-SREBPs treatments also induced the formation of caveolar or caveolae rosette structures compared to AdMT treatment (Fig. 2d). Thus, demonstrating the significant role of mechanosensing by SREBPs and excessive mechanotransduction upon activation in TM. Yet, quantitative changes in lamellipodia and filopodial like structures under AdSREBPs compared to the controls should be studied to identify if they participate in mechanosensing and mechanotransduction. This prompted us to examine the role of SREBPs in the regulation of IOP.

### 3.3 Pharmacological inactivation of SREBPs lowers IOP by altering the ECM architecture of the TM AH outflow pathway in *ex vivo* porcine perfusion cultures

After deriving a linear relationship between SREBPs activation, mechanosensing, and increased actin polymerization, we hypothesized that loss of SREBPs activity can have a significant effect on IOP. The pharmacological inhibition of SREBPs activity was accomplished using fatostatin [59]. Fatostatin treatment (20  $\mu$ M) for 24 h in PTM cells showed a significant decrease in N-SREBP1 ( $n = 4$ ,  $p = 0.01$ ) and N-SREBP2 ( $n = 4$ ,  $p = 0.02$ ) protein levels when assayed in the nuclear fraction (Fig. 3a) and in HTM cells significantly decreased N-SREBP1 ( $n = 4$ ,  $p = 0.03$ ) and N-SREBP2 ( $n = 4$ ,  $p = 0.0001$ ) in the total protein (Fig. 3b). The SCAP protein expression did not change ( $n = 4$ ,  $p = 0.3$ ) (Fig. 3b). 'n' here refers to the use of HTM cells as biological replicates of 4 cell strains. The IF localization of SREBP1 and SREBP2 distribution after fatostatin treatment demonstrated a marked decrease inside the nucleus compared to the controls (Fig. 3c and 3d). Histograms

on the right of Fig. 3c and 3d represent the ImageJ-based quantification of nuclear SREBPs fluorescent intensities showing a significant decrease in N-SREBP1 ( $n = 5$ ,  $p = 0.02$ ) and N-SREBP2 ( $n = 5$ ,  $p = 0.001$ ) fluorescent staining. 'n' here refers to the use of HTM cells as biological replicates of 2 cell strains with experimental replicates. Thus, providing the proof-of-concept for fatostatin inhibiting SREBPs activity in TM cells.

We then tested the effect of SREBPs inactivation via fatostatin on IOP *ex vivo* using the porcine organ culture system. Perfusion of 20  $\mu\text{M}$  fatostatin significantly decreased IOP by 12 h ( $n = 5$ ,  $p = 0.04$ ), and sustained until 22 h ( $n = 5$ ,  $p < 0.05$ ) (Fig. 3e) compared to the DMSO perfused control eyes. 'n' here refers to the number of porcine eyes used as biological replicates. To determine the effects of fatostatin on the TM outflow pathway structures, we analyzed the histological changes. Based on the H and E staining in the AH outflow pathway, the most prominent was the increased spacing between the TM (Fig. 3f) in the fatostatin perfused eyes compared to a more compact TM in the DMSO perfused eyes. As a proof of concept, post-perfusion immunoblotting on total protein from TM tissue showed significantly decreased N-SREBP1 ( $n = 4$ ,  $p = 0.005$ ) and N-SREBP2 ( $n = 4$ ,  $p = 0.03$ ) in fatostatin-perfused TM (Fig. 3g). Thus, demonstrating a direct result of SREBP inactivation on decreased IOP. Moreover, histochemical evaluation on the TM outflow pathway revealed both qualitative and quantitative decreases in ECM like COL1A and FN. We found that both COL1A and FN in the TM-JCT region showed a marked decrease compared to the control (Fig. 3h), which is represented in the histogram for COL1A staining ( $n = 5$ ,  $p = 0.0001$ ), and FN staining ( $n = 5$ ,  $p = 0.0001$ ) in the TM outflow pathway (Fig. 3h, right panel). To get better insights, we performed immunoblotting with the protein extracted from the TM tissue obtained from DMSO and fatostatin-perfused eyes. In agreement with IHC results, we found that compared to DMSO-perfused the fatostatin-perfused TM tissue showed significantly decreased expression of COL1A ( $n = 4$ ,  $p = 0.01$ ) and FN ( $n = 4$ ,  $p = 0.03$ ) (Fig. 3i). 'n' here refers to biological replicates used. Thereby, the direct inhibition of SREBPs activity significantly reduced IOP potentially by diminishing ECM in the TM outflow pathway and increasing the space around the TM tissue to increase the AH outflow.

### 3.4 Molecular inactivation of SREBPs by knocking down SCAP in *SCAP<sup>f/f</sup>* mice lowers IOP *in vivo*

Since we established the direct effect of SREBPs inactivation on IOP *ex vivo*, we checked the effect of SREBPs inactivation on IOP regulation in *SCAP<sup>f/f</sup>* mice *in vivo*. Conditional knockdown of SCAP was achieved using intravitreal injection of Ad5.CMV.iCre-eGFP in *SCAP<sup>f/f</sup>* mice inducing the loss of SCAP in the TM tissue due to Cre/lox recombination. The cohorts were divided into four groups - three injection groups: Ad5.CMV.iCre-eGFP, Ad5.CMV.eGFP (sham virus control), and saline (sham injection control) and one uninjected/untouched group. The IOP was measured over time in anesthetized *SCAP<sup>f/f</sup>* mice before injection to obtain the baseline IOP, and every 10 days after injection until 50 days post-injection. Data presented here show the mean IOP  $\pm$  SEM in mmHg. The Ad5.CMV.iCre-eGFP injection group displayed a significant IOP lowering ( $12.97 \pm 0.71$ ,  $n = 10$ ) compared to Ad5.CMV.eGFP injection group ( $21.74 \pm 1.47$ ,  $n = 9$ ,  $p = 0.0001$ ), saline injection group ( $20.5 \pm 1.00$ ,  $n = 10$ ,  $p = 0.0001$ ), and the untouched group ( $19.67 \pm 0.83$ ,  $n = 9$ ,  $p = 0.0001$ ) (Fig. 4a) 10 days after injection. The decreased IOP in Ad5.CMV.iCre-

eGFP injection group compared to the control groups sustained up to 30 days post-injection ( $n = 10$ ,  $p < 0.05$ ). At post-injection days 40 and 50, IOP in Ad5.CMV.iCre-eGFP injection group was significantly decreased ( $n = 10$ ,  $p < 0.05$ ) compared to saline injection and Ad5.CMV.eGFP injection groups. The IOP was also lower than the untouched group, but not statistically significant (Fig. 4a). We also compared the IOP changes within each group to their baseline normal IOP (before injection/time point 0 days), and the result shows that there was no significant change in IOP levels in untouched, saline injection, and Ad5.CMV.eGFP injection groups. However, within Ad5.CMV.iCre-eGFP injection group, the IOP was significantly decreased 10 days post-injection and sustained till 50 days post-injection ( $n = 10$ ,  $p < 0.05$ ). Start from 40 days post-injection, the IOP in Ad5.CMV.iCre-eGFP injection group was slowly went back to the baseline (Fig. 4b). Upon analyzing percentage changes in IOP (delta IOP %) in each group at each time point, Ad5.CMV.iCre-eGFP injection group showed a decrease of 40.38% compared to the baseline normal (before injection/time point 0 days) with an average decrease of 27.85% (Fig. 4c). The delta IOP % in the control groups were less than 13% changes of baseline normal IOP. (Fig. 4c). We evaluated IOP changes after SREBPs knock down in adult and old mice to check if aging in combination with SREBPs knockdown influenced IOP. We found IOP was consistently and significantly decreased in Ad5.CMV.iCre-eGFP group compared to Ad5.CMV.eGFP group ( $n = 5$ ,  $p < 0.05$ ), and it was also lower than the untouched group and saline injection group in the old and adult cohorts (Supplementary Fig. 5a and 5d, **respectively**). In both old and adult cohorts, there was no significant change in IOP levels in all sham control groups, but IOP was significantly decreased 10 days post-injection in Ad5.CMV.iCre-eGFP injection group and sustained till 50 days post-injection ( $n = 5$ ,  $p < 0.05$ ) (Supplementary Fig. 5b and 5e, **respectively**). The IOP in Ad5.CMV.iCre-eGFP injection groups showed a decrease of as much as 42.72 % and 43.14 % of baseline normal IOP in old and adult cohorts, respectively (Supplementary Fig. 5c and 5f, **respectively**). All sham control groups showed less than 17 % changes of baseline normal IOP in both old and adult mice (Supplementary Fig. 5c and 5f, **respectively**). ‘n’ here refers to number of mice used and since only one eye of the mice was injected, the number of eyes and mice are equal. At the end of the longitudinal IOP measurement study, the mice eyes were enucleated and processed for histological and IHC analysis. The H & E staining showed normal open iridocorneal angles and no marked differences in TM morphology in all the groups (Fig. 4d). Immunostaining in Ad5.CMV.iCre-eGFP injection group compared to all control groups for - SCAP showed a marked decrease in TM (Fig. 4e, green arrow in the inset), SREBP1 and SREBP2 showed decreased distribution in the nuclear regions in TM (Fig. 4f and 4g, green arrow in the inset). This data proves that selective molecular knockdown of SCAP in TM outflow pathway thereby inactivating SREBPs in TM significantly lowered IOP and confirmed the significance of SCAP-SREBP pathway in modulation of IOP.

### 3.5 SREBPs inactivation impacts lipid metabolism in TM

Since SREBPs are master regulators of lipid biosynthesis, as a proof-of-concept study, we looked at changes in lipid metabolism in HTM cells under fatostatin treatment. HTM cells treated with 20  $\mu\text{M}$  fatostatin for 24 h significantly decreased many of the SREBPs responsive mRNA expression (Fig. 5a) involved in - 1) genes related to cholesterol biosynthesis: low-density lipoprotein receptor (LDLR) ( $n = 4$ ,  $p = 0.002$ ),

hydroxymethylglutaryl-CoA synthase 1 (HMGCS1) (n = 4, p = 0.004), 3-Hydroxy-3-Methylglutaryl-CoA Reductase (HMGCR) (n = 4, p = 0.02), SREBP2 (n = 4, p = 0.02); 2) genes involved in fatty acid biosynthesis: acetyl-CoA carboxylase (ACC) (n = 4, p = 0.0007), fatty acid synthase (FAS) (n = 4, p = 0.0009), peroxisome proliferator-activated receptor gamma (PPARG) (n = 4, p = 0.005), acetyl-CoA synthetase (ACS) (n = 4, p = 0.0008), SREBP1 (n = 4, p = 0.0003); and 3) gene regulating triglyceride and phospholipid biosynthesis: glycerol-3-phosphate acyltransferase (GPAT) (n = 4, p = 0.08) (Fig. 5a). Using immunoblotting we checked for the expression of rate limiting enzymes involved in lipogenesis - FAS, HMGCR, and ACC under fatostatin treatment. Compared to the DMSO controls, fatostatin significantly decreased FAS (n = 4, p = 0.049), HMGCR (n = 4, p = 0.02), and ACC (n = 4, p = 0.049) expression (Fig. 5b). To further confirm the lipid changes under fatostatin treatment, we measured normalized phospholipid/cell, normalized free cholesterol/cell, and normalized triglyceride/cell. The results show that levels of phospholipid (n = 4, p = 0.0001) (Fig. 5c), free cholesterol (n = 4, p = 0.04) (Fig. 5d), and triglyceride (n = 4, p = 0.04) (Fig. 5e) were significantly reduced under fatostatin treatment. Interestingly the magnitude of the phospholipid decrease was the highest (~95%). 'n' here refers to HTM biological replicates used.

To better understand the detailed changes within each lipid class under SREBPs inactivation, we performed shotgun lipidomics post fatostatin treatment, which is a targeted metabolite analysis including phosphatidylcholine (PC), phosphatidylethanolamine (PE), phosphatidylserine (PS), cholesteryl ester (CE), fatty acids (FA), ceramide (Cer), sphingomyelin (SM), diacylglycerol (DG) and triglyceride (TG). As demonstrated in the volcano plot (Supplementary Fig. 6a), the lipids were presented as log 2-fold changes against the  $-\log_{10}(p)$  of the differential expression between the control (CTL) and fatostatin treatment (FATO). The analysis revealed 79 specific lipids above the threshold ( $|FC| > 1$ , and  $p < 0.05$ ), which were significantly changed in fatostatin treated HTM cells compared to DMSO treated control cells. The details of these 79 changed lipids are shown in the Table 3 and the heatmap features the top 80 lipids (Supplementary Fig. 6b). Based on the volcano analysis, fatostatin treatment significantly decreased mainly TG containing FA 14:0, DG, and PS. Fatostatin treatment also significantly increased some lipids, mainly including TG containing FA 16:0 and FA 18:0, alkyl-PC, and plasmenyl-PC, which are ether phospholipids. This finding suggests that SREBPs inactivation not only disturbs lipid biosynthesis but also modulates the metabolism of lipid subclasses. Looking at the KEGG human pathways (Table 4) based on total lipids changes we found that major pathways affected due to fatostatin treatment were glycosylphosphatidylinositol (GPI)-anchor biosynthesis, glycerophospholipid metabolism, arachidonic acid metabolism, linoleic acid metabolism, alpha-linoleic acid metabolism, biosynthesis of unsaturated fatty acids, sphingolipid metabolism, and steroid biosynthesis. Together, this demonstrates that SREBPs inactivation using fatostatin lowers lipid biosynthesis in HTM cells by decreasing the expression of SREBPs responsive genes. Further, emphasizing the potential role of lipids regulated by SREBPs in regulating IOP.

### 3.6 SREBPs inactivation aids in the induction of cellular relaxation and focal adhesion signaling

Since activation of SREBPs induced contractile phenotype in the cells, our logical step was to check if SREBPs inactivation by fatostatin modulated actin polymerization and FA based cellular tension. We probed for F-actin using phalloidin labeling in HTM cells along with FA proteins – vinculin and paxillin. As seen in Fig. 6a and 6b, compared to DMSO control, 24 h of 20  $\mu$ M fatostatin treatment on HTM cells demonstrated a marked decrease in the F-actin stress fibers (green staining in merged/grayscale) and sparse distribution of vinculin and paxillin at the edges of F-actin fibers with greater cytoplasmic accumulation (red staining in the merged/grayscale, indicated by white arrows). To further confirm this result, we extracted F-actin and globular actin (G-actin) from control and fatostatin-treated HTM cells separately and checked the changes in F-actin/G-actin ratio in each condition. Fig. 6c shows that fatostatin significantly decreased F-actin/G-actin ratio ( $n = 4$ ,  $p = 0.04$ ), implying the decreased actin polymerization under fatostatin treatment. Since changes in actin polymerization affect cell contractility, we next assayed for the p-MLC/MLC ratio. Immunoblotting of the fatostatin treated protein lysate showed a significant decrease in the ratio of p-MLC/MLC ratio ( $n = 4$ ,  $p = 0.002$ ) (Fig. 6d), indicating that SREBPs inactivation can reduce HTM cell contractility. Finally, we examined the expression of proteins involved in FA formation, F-actin polymerization, and their stabilization. Fascin is a major F-actin bundling protein and regulates the maintenance and stability of parallel bundles of F-actin in various cell types including TM [68],[23]. Immunoblotting showed that fatostatin significantly decreased fascin-1 levels ( $n = 4$ ,  $p = 0.03$ ) (Fig. 6e) with no change in vinculin levels ( $n = 4$ ,  $p = 0.6$ ) (Fig. 6e). Suggesting that fatostatin destabilized the vinculin distribution at the edge of F-actin fibers, but not vinculin levels. We found that fatostatin significantly decreased levels of LIM kinase 1 (LIMK1) ( $n = 4$ ,  $p = 0.04$ ) (Fig. 6e), an actin polymerization and stabilization protein [69]. Looking at cofilin, we found no significant change in the levels of total-cofilin (T-cofilin) ( $n = 4$ ,  $p = 0.3$ ), but phosphorylated cofilin at serine 3 (P-cofilin) ( $n = 4$ ,  $p = 0.003$ ) and the ratio of P-cofilin/T-cofilin was significantly decreased in fatostatin treatment ( $n = 4$ ,  $p = 0.004$ ) (Fig. 6f). Therefore, providing evidence for weakening the LIMK1-cofilin-driven actin polymerization. Moreover, we also found that fatostatin treatment increased total-paxillin (T-paxillin) levels ( $n = 4$ ,  $p = 0.07$ ), and significantly decreased its tyrosine 118 phosphorylated form (P-paxillin) ( $n = 4$ ,  $p = 0.03$ ). The ratio of P-paxillin/T-paxillin was significantly decreased in fatostatin treatment ( $n = 4$ ,  $p = 0.01$ ) (Fig. 6g). 'n' here refers to HTM biological replicates used. Thus indicating decreased cellular contractility and cell adhesive interactions due to SREBPs inactivation.

### 3.7 SREBPs activation is a critical regulator of ECM engagement to the matrix sites

Alterations in actin and focal adhesions can have a direct impact on ECM adhesion [70]. We found that inhibition of SCAP-SREBP pathway using fatostatin (20  $\mu$ M for 24 h) significantly decreased all ECM mRNA expression, including FN ( $n = 4$ ,  $p = 0.03$ ), COL1a ( $n = 4$ ,  $p = 0.0004$ ), COL6a ( $n = 4$ ,  $p = 0.01$ ), COL4a ( $n = 4$ ,  $p = 0.002$ ), tenascin C (TNC) ( $n = 4$ ,  $p = 0.03$ ), transforming growth factor  $\beta$ 2 (TGF $\beta$ 2) ( $n = 4$ ,  $p = 0.0003$ ), and sarcospan (SSPN) ( $n = 4$ ,  $p = 0.002$ ) (Fig. 7a). Consequently, upon fatostatin treatment, the whole cell lysate (CL) protein expression analysis showed a significant reduction of FN ( $n = 4$ ,  $p = 0.01$ ) and COL1A ( $n = 4$ ,  $p = 0.001$ ) (Fig. 7b). In addition, secretory ECM



levels FN ( $n = 4$ ,  $p = 0.02$ ) and COL1A ( $n = 4$ ,  $p = 0.001$ ) in conditioned media (CM) was significantly decreased (Fig. 7c). 'n' here refers to biological replicates used. These results were confirmed using IF, where FN (Fig. 7d) and COL1A (Fig. 7e) immunolabeling were robustly decreased.

Finally, to discern the role of SREBPs activation in the regulation of ECM recruitment to the matrix sites, IF was performed for ECM like FN and COL1A (Fig. 7f and 7g, green staining) under the expression of constitutively active SREBP1a or 1c or 2 with the endogenous total SREBP activity inhibited using fatostatin (20  $\mu$ M for 24 h). The lower magnification images of the cells can be visualized in the Supplementary Fig. 7, with the box indicating the cells chosen for detailed explanation in Fig. 7f and 7g. In a compelling manner, the presence of Ad5-N-SREBP1a (Fig. 7f, second-row third column), Ad5-N-SREBP1c (Fig. 7f, third-row third column), and Ad5-N-SREBP2 (Fig. 7f, fourth-row third column) induced higher FN perinuclear distribution inside the cell (denoted by yellow arrows) compared to the AdMT control (Fig. 7f, first-row third column). Similar pattern was observed for COL1A. Compared to AdMT combined with fatostatin treatment (Fig. 7g, first-row third column), Ad5-N-SREBP1a (Fig. 7g, second-row third column), Ad5-N-SREBP1c (Fig. 7g, third-row third column), and Ad5-N-SREBP2 (Fig. 7g, fourth-row third column) combined with fatostatin treatment caused higher COL1A distribution inside the cells, and more COL1A puncta mostly located near the cell membrane (denoted by yellow arrows). We also observed a stronger COL1A fibril formation in Ad5-N-SREBP1a (Fig. 7g, second-row third column). The observed phenomenon described above was seen in 88 cells of the total 160 cells (55%) analyzed from three slides in three different donor lines.

Therefore, put together this data defines that SREBPs activation is indispensable for ECM production, trafficking, and engagement to the matrix sites.

#### 4. Discussion:

This study provides the first detailed evidence of the mechanosensing and mechanotransduction role of SREBPs in TM. We have further established the cellular and molecular basis for the SREBPs activation under increased mechanical stress in TM [41]. Mechanosensing is an important function of TM [71, 72] to maintain the IOP homeostasis [73] and excessive mechanotransduction in TM outflow pathway can result in increased TM cell tension and stiffness [25, 74]. Such changes have been documented in experimental models of glaucoma [75] and in human glaucomatous TM [76]. Moreover, increased stiffness can lead to loss in mechanosensing function of the TM AH outflow pathway [77]. Here, we have established the positive feedforward loop connecting mechanical stress to actin-based contractility via SREBP activation. The TM adapts to increased mechanical stress by modifying the actin cytoskeleton and the ECM [41, 67]. Augmenting SREBPs activation, induced contractility indicating a perpetual feedforward signaling from mechanical stress sensing by SREBPs resulting in induction of contractile force in the TM. Our study also demonstrates that inhibiting SREBPs activation mitigates mechanical stress-induced actin stress fiber formation providing a strong basis for SREBPs acting as mechanosensors and mechanotransducers. In fact, studies in cancer lines and *Drosophila* have demonstrated that acto-myosin contractility and mechanical forces imposed by the

ECM can regulate SREBP1 [51]. Interestingly, along with the mechanosensing function of SREBPs in TM and the expression and distribution of SREBPs and SCAP in the TM-JCT outflow pathway compared to other tissues of the ocular anterior segment suggested a potential role in IOP regulation. Likewise, we provide *ex vivo* and *in vivo* based evidence to show that SREBPs activity might play an important role in the maintenance of IOP. Both pharmacological and molecular inactivation of SREBPs significantly lowered IOP. We believe that the effect of inhibiting a transcription factor will require a longer time to produce the effect but will be longer lasting. We predict this because SREBPs inactivation will require regulation at the gene expression level first followed by changes in protein/enzyme levels and finally effecting physiological changes. Moreover, since anterior segment perfusion technique utilizes constant inflow, this also directly proves that the IOP lowering is potentially by increasing the AH drainage via the TM outflow pathway. Additionally, *in vivo* studies in *SCAP<sup>ff</sup>* mice injected with Ad5.CMV.iCre-eGFP confirmed that the molecular inactivation of SREBPs by knocking down SCAP significantly lowered IOP by 10 days post-injection. Further studies to understand the role of SCAP-SREBP pathway in the SC and the distal outflow pathways will be extremely significant. Studies on AH dynamics *in vivo* after inactivation or constitutively activating SREBPs can provide additional insights into AH drainage modalities. Despite available IOP-lowering drugs, there remains an unmet need for novel, efficacious, and mechanism-based targeted therapy for ocular hypertension and POAG with minimal side effects [78]. Testing the pharmacological inactivation of SREBPs on IOP in animal models can help us identify novel topical drugs to lower IOP. Curiously, there is evidence that SREBP1 activation and increased lipogenesis results in cellular senescence [79]. Interestingly in aging and glaucoma, it has been proposed that there is a gradual loss of TM cellularity [80, 81]. It will be key to unravel the role of SREBP isoforms – SREBP1 and SREBP2 - and their activation paradigm in TM during aging, to elucidate the resultant effects on TM cellularity and IOP, and in the onset and progression of glaucoma pathogenesis.

The major function of SREBPs is regulating lipogenesis [45]. In line, upon inactivation of the SCAP-SREBP pathway, we found a significant decrease in total TM phospholipids (~90%) as well as in cholesterol and triglycerides. In addition, our lipidomic analysis showed that multiple lipid subclasses were modified after SREBPs inactivation using fatostatin. Interestingly, among the 79 significantly changed lipids, TG containing FA 14:0 was significantly decreased, but TG containing FA 16:0 and 18:0 were significantly increased. Although serum total TG levels have been found to be related to the risk of increased IOP and POAG [82–84] the FA composition of TG in TM has never been studied before. These differential changes within the TG subclasses in TM may suggest different properties and functions of TG subclasses in TM biomechanics. We also found that some phospholipid subclasses - alkyl-PC and plasmeyl-PC were significantly increased after fatostatin treatment. Both alkyl-PC and plasmeyl-PC belong to ether phospholipids, a major structural component of cell membranes. Even though ether phospholipids have never been studied in TM cells, studies in other cell types reveal that ether phospholipids can regulate cell membrane dynamics, membrane trafficking, and cell signaling such as PPARG and Akt, and play an antioxidant role [85, 86]. In addition, decrease in ether phospholipids is associated with hypertension [87, 88]. Such changes in ether phospholipids

in TM cells further demonstrate that SREBPs inactivation can modulate lipid compositions on the TM cell membrane and affect membrane structures and signaling pathways. Current understanding of the correlation between the regulation of lipid levels in the TM outflow pathway with IOP changes is unclear. Lipids levels are known to be varied in AH from ocular hypertensives and can participate in the pathogenesis of elevated IOP [32, 89–91]. Some well-studied lipids contributing to ocular hypertension are the bioactive lysophospholipids (lipid growth factors) [33, 92–95], and cholesterol [34–36]. Yet the causality has not been completely attributed to increased lipids on IOP elevation. Based on recent epidemiologic studies, there is an association between cholesterol and glaucoma, although the findings have not been conclusive if hyperlipidemia is a cause or an effect of the disease. Some studies found that hyperlipidemia, especially high cholesterol levels, is significantly associated with an increased risk of glaucoma and increased IOP [35, 36, 96] [97] and others show the opposite [98] [99]. Interestingly, even though it is not clear how cholesterol is related to the glaucoma risk, there is mounting evidence showing that HMG-CoA reductase inhibitor statin can decrease POAG risk by mitigating disease progression [38, 100, 101]. The proposed mechanism for statins to decrease IOP is by inhibiting the isoprenylation of Rho GTPase thus resulting in decreased actomyosin contractile activity and ECM synthesis/assembly [39, 102–104]. All these studies imply that there is an association between lipids, ocular hypertension, and POAG. The data we show clearly suggests that inactivating SCAP-SREBP pathway decreases TM lipids. Thus, connecting the aspects of lowering lipids leading to IOP lowering. However, the contributions of lipid metabolism in TM for the regulation of TM biomechanics and IOP are blurred [105]. We have recently identified that TM cholesterol plays a significant role in the maintenance of the polymerized state of actin, FA recruitment, and TM membrane tension (*Unpublished study*). Thus, suggesting a strong contribution of lipids including cholesterol in regulating TM actin-adhesion complex-ECM modulated via the SCAP-SREBP pathway to efficiently regulate IOP changes and potential participation in achieving IOP homeostasis.

This study strengthens the correlation between lipid changes and tissue stiffness and reinforces the significance and role of actin-cell adhesive interactions in bringing about changes in IOP [106]. It has been characterized that the FA vinculin but not paxillin directly interacts with actin [107, 108]. Additional mechanistic evidence in our study confirms that SREBPs inactivation regulates vinculin distribution but not expression confirming the requirement of SREBPs activity in modulating the recruitment of vinculin to the FA site. Also, a decrease in paxillin phosphorylation suggests a decreased inside-out signaling towards integrin binding to ECM and recruitment of FA [109, 110]. Inside the cells, we identified that loss of SREBPs activation lowered the actin-bundling protein fascin-1 [23, 68, 111]. The decreased fascin-1 expression under fatostatin treatment can result in a slower rate of actin polymerization with lesser filopodia formation [112, 113]. Within this context, the decreased LIMK1 resulting in the loss of phosphorylation of cofilin-1 at serine 3 can induce F-actin destabilization and this can prevent contraction and attenuate hypertension [69, 114]. Thus, we propose that the loss of cell adhesive interaction upon SREBPs inactivation is an important mechanism in lowering the IOP. Interestingly, we found that there was a strong negative regulation of most of the ECM gene expression upon fatostatin treatment in HTM cells. Though it is not yet clear if SREBPs directly regulate the transcription of

ECM genes, we believe this to be a result of negative feedback outside-in signaling towards transcribing ECM genes due to the disengagement of ECM. *Ex vivo* evidence indicated a significant loss in the ECM components like collagen and fibronectin in the outflow pathway which concurred in the *in vitro* experiments in HTM cells. *In vitro* analysis provided further proof that the inactivation of SREBPs decreased actin fibers and increased retraction of FAs to the cytosol with very little found at the edges of the cells. The FAs aid in linking the intracellular cytoskeleton to the extracellular ECM [115]. A compromise in vinculin and paxillin localization at the edge of F-actin fibers dictates the dissolution of FAs and decreased cell-ECM connections. Put together, the SCAP-SREBP inactivation induced TM relaxation and ECM-based stiffness potentially by downregulating lipogenesis resulting in IOP decrease.

Finally, of significant interest is the role of SREBPs activation in regulating the ECM engagement to the membrane potentially for the release, modification, and cross-linking. This could be due to the cellular and membrane lipid changes resulting from SREBPs activation. Additionally, we found marked changes in the caveolar structures including the rosette formation upon SREBPs activation. These structures could be involved in mechanosensing, mechanotransduction, possibly to mitigate mechanical stress, and to buffer membrane tension [116–118]. Moreover, multiple rate-limiting enzymes in lipid biogenic pathways like FAS [52, 119], ACC [120, 121], HMGCR, and SREBPs are implicated in increasing ECM and fibrosis in various tissue types [122–124]. ACC catalyzes the carboxylation of acetyl-CoA into malonyl-CoA. This reaction is the first and the rate-limiting step in the biosynthesis of fatty acids. Significantly, acetyl-CoA metabolism is implicated in POAG [125]. Further investigation on the role of these rate limiting enzymes in controlling the metabolism and TM biomechanics is essential to decode their function in IOP regulation. Though out of scope for this manuscript, we predict that SREBPs can modulate ECM remodeling via lipid-independent pathways. SREBP1 has been shown to bind to the promoter region of TGF $\beta$  [126], a major pro-fibrotic factor. Also, SREBP1 can act as a cell surface retention factor for the TGF $\beta$  receptor, T $\beta$ RI, by preventing its secretion in exosomes or directly changing COL VI transcription [127] [128]. Thus, pointing to the idea that SREBPs activation can increase ECM production and deposition and IOP elevation in both lipid-dependent and -independent pathways. Therefore, identifying all the gene promoters that SREBPs bind to in TM genome and teasing out the lipid-dependent and -independent pathways responsible for modulating actin dynamics and ECM remodeling in TM is essential.

## 5. Conclusion

In summary, this study presents a novel way of lowering IOP by inactivating SREBPs through decreasing lipogenesis, actin-based tension, and attenuating ECM accumulation in TM (**Graphical Abstract - Created using Biorender.com**). Thus, demonstrating the important role of SREBPs in mechanosensing and mechanotransduction in TM to regulate contractility and stiffness, and IOP regulation. Further understanding on other modalities of SREBPs regulating the actin cytoskeleton and ECM in TM will aid in identifying better targets for IOP lowering and glaucoma therapy.

## Supplementary Material

Refer to Web version on PubMed Central for supplementary material.

## Acknowledgments

We acknowledge Dr. Nuria Morral, Dr. Benjamin Perrin, Dr. Gary Landreth, and Dr. Tim Corson from IUSM for their useful discussions on the project. Derrick Gray from Center for Electron Microscopy (iCEM) and Instrumentation grant from the NIH - 1S10OD028723 to iCEM. We thank Dr. Christina Ferreira from the Bindley Bioscience Center, Purdue University, for the discussions, planning, and help with the execution of the MRM-based Lipidomics analysis, and data analysis.

## Funding

This project was supported by the National Institutes of Health/ National Eye Institute (R01EY029320) (PPP), R01DK124343 (TO), Glick Research Endowment Funds (PPP), Cohen AMD Research Pilot Grant (PPP), RPB Departmental Pilot Grant (PPP), Sigma Xi Grant-in-aid (TW), and Challenge grant from Research to Prevent Blindness to IU.

## Disclosures

The authors declare that they have no conflict of interest. The funders had no role in the design of the study; in the collection, analyses, or interpretation of data; in the writing of the manuscript, or in the decision to publish the results.

## Data availability statement

The datasets presented in this study is available upon request from the corresponding author.

## References

- [1]. Weinreb RN and Khaw PT, "Primary open-angle glaucoma," *Lancet*, Research Support, Non-U.S. Gov't Research Support, U.S. Gov't, P.H.S. Review vol. 363, no. 9422, pp. 1711–20, May 22 2004, doi: 10.1016/S0140-6736(04)16257-0. [PubMed: 15158634]
- [2]. Grant WM, "Clinical tonography," *Trans Am Acad Ophthalmol Otolaryngol*, vol. 55, pp. 774–81, Nov-Dec 1951. [Online]. Available: <https://www.ncbi.nlm.nih.gov/pubmed/14893332>. [PubMed: 14893332]
- [3]. Grant WM, "Experimental aqueous perfusion in enucleated human eyes," *Arch Ophthalmol*, vol. 69, pp. 783–801, Jun 1963. [Online]. Available: <https://www.ncbi.nlm.nih.gov/pubmed/13949877>. [PubMed: 13949877]
- [4]. Sharif NA, "Therapeutic Drugs and Devices for Tackling Ocular Hypertension and Glaucoma, and Need for Neuroprotection and Cytoprotective Therapies," *Frontiers in pharmacology*, vol. 12, p. 729249, 2021, doi: 10.3389/fphar.2021.729249.
- [5]. Shiose Y, "Intraocular pressure: new perspectives," *Surv Ophthalmol*, vol. 34, no. 6, pp. 413–35, May-Jun 1990. [Online]. Available: <http://www.ncbi.nlm.nih.gov/pubmed/2194306>. [PubMed: 2194306]
- [6]. Bonomi L et al. , "Prevalence of glaucoma and intraocular pressure distribution in a defined population. The Egna-Neumarkt Study," *Ophthalmology*, vol. 105, no. 2, pp. 209–15, Feb 1998. [Online]. Available: <http://www.ncbi.nlm.nih.gov/pubmed/9479277>. [PubMed: 9479277]
- [7]. Dielemans I, Vingerling JR, Algra D, Hofman A, Grobbee DE, and de Jong PT, "Primary open-angle glaucoma, intraocular pressure, and systemic blood pressure in the general elderly population. The Rotterdam Study," *Ophthalmology*, vol. 102, no. 1, pp. 54–60, Jan 1995. [Online]. Available: <http://www.ncbi.nlm.nih.gov/pubmed/7831042>. [PubMed: 7831042]
- [8]. Quigley HA, "Open-angle glaucoma," (in eng), *The New England journal of medicine*, vol. 328, no. 15, pp. 1097–106, Apr 15 1993, doi: 10.1056/NEJM199304153281507. [PubMed: 8455668]

- [9]. Saaddine JB, Narayan KM, and Vinicor F, "Vision loss: a public health problem?," *Ophthalmology*, vol. 110, no. 2, pp. 253–4, Feb 2003. [Online]. Available: <https://www.ncbi.nlm.nih.gov/pubmed/12578764>. [PubMed: 12578764]
- [10]. Tham YC, Li X, Wong TY, Quigley HA, Aung T, and Cheng CY, "Global prevalence of glaucoma and projections of glaucoma burden through 2040: a systematic review and meta-analysis," *Ophthalmology*, vol. 121, no. 11, pp. 2081–90, Nov 2014, doi: 10.1016/j.ophtha.2014.05.013. [PubMed: 24974815]
- [11]. Quigley HA and Broman AT, "The number of people with glaucoma worldwide in 2010 and 2020," *British journal of ophthalmology*, vol. 90, no. 3, pp. 262–267, 2006. [PubMed: 16488940]
- [12]. Kass MA et al., "The Ocular Hypertension Treatment Study: a randomized trial determines that topical ocular hypotensive medication delays or prevents the onset of primary open-angle glaucoma," *Arch Ophthalmol, Research Support, U.S. Gov't, P.H.S.* vol. 120, no. 6, pp. 701–13; discussion 829–30, Jun 2002. [Online]. Available: <http://www.ncbi.nlm.nih.gov/pubmed/12049574>. [PubMed: 12049574]
- [13]. Clark AF and Yorio T, "Ophthalmic drug discovery," (in eng), *Nat Rev Drug Discov*, vol. 2, no. 6, pp. 448–59, Jun 2003, doi: 10.1038/nrd1106nrd1106[pii]. [PubMed: 12776220]
- [14]. Lee AJ and Goldberg I, "Emerging drugs for ocular hypertension.," (in English), *Expert Opin Emerg Drugs, Review* vol. 16, no. 1, pp. 137–161, Apr 2011, doi: 10.1517/14728214.2011.521631. [PubMed: 21352074]
- [15]. Crawley L, Zamir SM, Cordeiro MF, and Guo L, "Clinical options for the reduction of elevated intraocular pressure," *Ophthalmol Eye Dis*, vol. 4, pp. 43–64, 2012, doi: 10.4137/OED.S4909. [PubMed: 23650457]
- [16]. Sunderland DK and Sapra A, "Physiology, Aqueous Humor Circulation," in *StatPearls. Treasure Island (FL)*, 2022.
- [17]. Wiederholt M, Schafer R, Wagner U, and Lepple-Wienhues A, "Contractile response of the isolated trabecular meshwork and ciliary muscle to cholinergic and adrenergic agents," *Ger J Ophthalmol*, vol. 5, no. 3, pp. 146–53, May 1996. [Online]. Available: <https://www.ncbi.nlm.nih.gov/pubmed/8803576>. [PubMed: 8803576]
- [18]. Stumpff F and Wiederholt M, "Regulation of trabecular meshwork contractility," *Ophthalmologica. Journal international d'ophtalmologie. International journal of ophthalmology. Zeitschrift fur Augenheilkunde, Research Support, Non-U.S. Gov't Review* vol. 214, no. 1, pp. 33–53, Jan-Feb 2000, doi: 10.1159/000027471.
- [19]. Wiederholt M, Thieme H, and Stumpff F, "The regulation of trabecular meshwork and ciliary muscle contractility," *Prog Retin Eye Res, Research Support, Non-U.S. Gov't Review* vol. 19, no. 3, pp. 271–95, May 2000, doi: 10.1016/s1350-9462(99)00015-4. [PubMed: 10749378]
- [20]. Stamer WD, "The cell and molecular biology of glaucoma: mechanisms in the conventional outflow pathway," *Invest Ophthalmol Vis Sci*, vol. 53, no. 5, pp. 2470–2, May 4 2012, doi: 10.1167/iovs.12-9483f. [PubMed: 22562843]
- [21]. Abu-Hassan DW, Acott TS, and Kelley MJ, "The Trabecular Meshwork: A Basic Review of Form and Function," *J Ocul Biol*, vol. 2, no. 1, May 2014, doi: 10.13188/2334-2838.1000017.
- [22]. Carreon T, van der Merwe E, Fellman RL, Johnstone M, and Bhattacharya SK, "Aqueous outflow - A continuum from trabecular meshwork to episcleral veins," (in eng), *Prog Retin Eye Res*, vol. 57, pp. 108–133, Mar 2017, doi: 10.1016/j.preteyeres.2016.12.004. [PubMed: 28028002]
- [23]. Soundararajan A, Ghag SA, Vuda SS, Wang T, and Pattabiraman PP, "Cathepsin K Regulates Intraocular Pressure by Modulating Extracellular Matrix Remodeling and Actin-Bundling in the Trabecular Meshwork Outflow Pathway," *Cells*, vol. 10, no. 11, p. 2864, Oct 24 2021, doi: 10.3390/cells10112864. [PubMed: 34831087]
- [24]. Pattabiraman PP and Toris CB, "The exit strategy: Pharmacological modulation of extracellular matrix production and deposition for better aqueous humor drainage," *Eur J Pharmacol*, vol. 787, pp. 32–42, Sep 15 2016, doi: 10.1016/j.ejphar.2016.04.048. [PubMed: 27112663]
- [25]. Pattabiraman PP, Rinkoski T, Poeschla E, Proia A, Challa P, and Rao PV, "RhoA GTPase-induced ocular hypertension in a rodent model is associated with increased fibrogenic activity in the

trabecular meshwork,” *The American journal of pathology*, vol. 185, no. 2, pp. 496–512, Feb 2015, doi: 10.1016/j.ajpath.2014.10.023. [PubMed: 25499974]

- [26]. Wang K, Read AT, Sulchek T, and Ethier CR, “Trabecular meshwork stiffness in glaucoma,” *Exp Eye Res*, vol. 158, pp. 3–12, May 2017, doi: 10.1016/j.exer.2016.07.011. [PubMed: 27448987]
- [27]. Vranka JA, Kelley MJ, Acott TS, and Keller KE, “Extracellular matrix in the trabecular meshwork: intraocular pressure regulation and dysregulation in glaucoma,” (in eng), *Exp Eye Res*, vol. 133, pp. 112–25, Apr 2015, doi: 10.1016/j.exer.2014.07.014. [PubMed: 25819459]
- [28]. Tamm ER, Braunger BM, and Fuchshofer R, “Intraocular Pressure and the Mechanisms Involved in Resistance of the Aqueous Humor Flow in the Trabecular Meshwork Outflow Pathways,” (in eng), *Prog Mol Biol Transl Sci*, vol. 134, pp. 301–14, 2015, doi: 10.1016/bs.pmbts.2015.06.007. [PubMed: 26310162]
- [29]. Liu P, Wang F, Song Y, Wang M, and Zhang X, “Current situation and progress of drugs for reducing intraocular pressure,” (in eng), *Therapeutic advances in chronic disease*, vol. 13, p. 20406223221140392, 2022, doi: 10.1177/20406223221140392.
- [30]. Humphrey JD, Dufresne ER, and Schwartz MA, “Mechanotransduction and extracellular matrix homeostasis,” (in eng), *Nature reviews. Molecular cell biology*, vol. 15, no. 12, pp. 802–812, 2014, doi: 10.1038/nrm3896. [PubMed: 25355505]
- [31]. Azbukina NV et al. , “Targeted Lipidomic Analysis of Aqueous Humor Reveals Signaling Lipid-Mediated Pathways in Primary Open-Angle Glaucoma,” *Biology (Basel)*, vol. 10, no. 7, p. 658, Jul 13 2021, doi: 10.3390/biology10070658. [PubMed: 34356513]
- [32]. Edwards G, Arcuri J, Wang H, Ziebarth N, Zode G, Lee RK, and Bhattacharya SK, “Endogenous ocular lipids as potential modulators of intraocular pressure,” (in eng), *J Cell Mol Med*, vol. 24, no. 7, pp. 3856–3900, Apr 2020, doi: 10.1111/jcmm.14975. [PubMed: 32090468]
- [33]. Rao PV, “Bioactive lysophospholipids: role in regulation of aqueous humor outflow and intraocular pressure in the context of pathobiology and therapy of glaucoma,” *J Ocul Pharmacol Ther*, vol. 30, no. 2–3, pp. 181–90, Mar-Apr 2014, doi: 10.1089/jop.2013.0194. [PubMed: 24283588]
- [34]. Madjedi KM et al. , “The Association between Serum Lipids and Intraocular Pressure in 2 Large United Kingdom Cohorts,” (in eng), *Ophthalmology*, vol. 129, no. 9, pp. 986–996, Sep 2022, doi: 10.1016/j.ophtha.2022.04.023. [PubMed: 35500606]
- [35]. Posch-Pertl L, Michelitsch M, Wagner G, Wildner B, Silbernagel G, Pregartner G, and Wedrich A, “Cholesterol and glaucoma: a systematic review and meta-analysis,” *Acta Ophthalmol*, vol. 100, no. 2, pp. 148–158, Mar 2022, doi: 10.1111/aos.14769. [PubMed: 33506616]
- [36]. Wang S and Bao X, “Hyperlipidemia, Blood Lipid Level, and the Risk of Glaucoma: A Meta-Analysis,” (in eng), *Invest Ophthalmol Vis Sci*, vol. 60, no. 4, pp. 1028–1043, Mar 1 2019, doi: 10.1167/iops.18-25845. [PubMed: 30897618]
- [37]. Marcus MW et al. , “Cholesterol-lowering drugs and incident open-angle glaucoma: a population-based cohort study,” *PloS one*, vol. 7, no. 1, p. e29724, 2012, doi: 10.1371/journal.pone.0029724. [PubMed: 22238644]
- [38]. Stein JD, Newman-Casey PA, Talwar N, Nan B, Richards JE, and Musch DC, “The relationship between statin use and open-angle glaucoma,” *Ophthalmology*, vol. 119, no. 10, pp. 2074–81, Oct 2012, doi: 10.1016/j.ophtha.2012.04.029. [PubMed: 22727176]
- [39]. Song J, Deng PF, Stinnett SS, Epstein DL, and Rao PV, “Effects of cholesterol-lowering statins on the aqueous humor outflow pathway,” *Invest Ophthalmol Vis Sci*, vol. 46, no. 7, pp. 2424–32, Jul 2005, doi: 10.1167/iops.04-0776. [PubMed: 15980231]
- [40]. Von Zee CL, Richards MP, Bu P, Perlman JI, and Stubbs EB Jr., “Increased RhoA and RhoB protein accumulation in cultured human trabecular meshwork cells by lovastatin,” *Invest Ophthalmol Vis Sci*, vol. 50, no. 6, pp. 2816–23, Jun 2009, doi: 10.1167/iops.08-2466. [PubMed: 19151402]
- [41]. Soundararajan A et al. , “Multiomics analysis reveals the mechanical stress-dependent changes in trabecular meshwork cytoskeletal-extracellular matrix interactions,” (in English), *Front Cell Dev Biol*, Original Research vol. 10, p. 874828, 2022-September-13 2022, doi: 10.3389/fcell.2022.874828. [PubMed: 36176278]

- [42]. Shimano H and Sato R, “SREBP-regulated lipid metabolism: convergent physiology - divergent pathophysiology,” *Nat Rev Endocrinol*, vol. 13, no. 12, pp. 710–730, Dec 2017, doi: 10.1038/nrendo.2017.91. [PubMed: 28849786]
- [43]. Shimano H, “Sterol regulatory element-binding proteins (SREBPs): transcriptional regulators of lipid synthetic genes,” (in eng), *Prog Lipid Res*, vol. 40, no. 6, pp. 439–52, Nov 2001, doi: 10.1016/s0163-7827(01)00010-8. [PubMed: 11591434]
- [44]. Eberle D, Hegarty B, Bossard P, Ferre P, and Foufelle F, “SREBP transcription factors: master regulators of lipid homeostasis,” *Biochimie*, vol. 86, no. 11, pp. 839–48, Nov 2004, doi: 10.1016/j.biochi.2004.09.018. [PubMed: 15589694]
- [45]. Horton JD, Goldstein JL, and Brown MS, “SREBPs: activators of the complete program of cholesterol and fatty acid synthesis in the liver,” (in eng), *J Clin Invest*, vol. 109, no. 9, pp. 1125–31, May 2002, doi: 10.1172/jci15593. [PubMed: 11994399]
- [46]. Goldstein JL, DeBose-Boyd RA, and Brown MS, “Protein sensors for membrane sterols,” *Cell*, vol. 124, no. 1, pp. 35–46, Jan 13 2006, doi: 10.1016/j.cell.2005.12.022. [PubMed: 16413480]
- [47]. Dorotea D, Koya D, and Ha H, “Recent Insights Into SREBP as a Direct Mediator of Kidney Fibrosis via Lipid-Independent Pathways,” *Front Pharmacol*, vol. 11, p. 265, 2020, doi: 10.3389/fphar.2020.00265. [PubMed: 32256356]
- [48]. Matsuda M et al. , “SREBP cleavage-activating protein (SCAP) is required for increased lipid synthesis in liver induced by cholesterol deprivation and insulin elevation,” *Genes Dev*, vol. 15, no. 10, pp. 1206–16, May 15 2001, doi: 10.1101/gad.891301. [PubMed: 11358865]
- [49]. Sakai J, Nohturfft A, Goldstein JL, and Brown MS, “Cleavage of sterol regulatory element-binding proteins (SREBPs) at site-1 requires interaction with SREBP cleavage-activating protein. Evidence from in vivo competition studies,” *J Biol Chem*, vol. 273, no. 10, pp. 5785–93, Mar 6 1998, doi: 10.1074/jbc.273.10.5785. [PubMed: 9488713]
- [50]. Daemen S, Kutmon M, and Evelo CT, “A pathway approach to investigate the function and regulation of SREBPs,” *Genes Nutr*, vol. 8, no. 3, pp. 289–300, May 2013, doi: 10.1007/s12263-013-0342-x. [PubMed: 23516131]
- [51]. Bertolio R et al. , “Sterol regulatory element binding protein 1 couples mechanical cues and lipid metabolism,” *Nat Commun*, vol. 10, no. 1, p. 1326, Mar 22 2019, doi: 10.1038/s41467-019-09152-7. [PubMed: 30902980]
- [52]. Zhao X, Kwan JYY, Yip K, Liu PP, and Liu FF, “Targeting metabolic dysregulation for fibrosis therapy,” (in eng), *Nat Rev Drug Discov*, vol. 19, no. 1, pp. 57–75, Jan 2020, doi: 10.1038/s41573-019-0040-5. [PubMed: 31548636]
- [53]. Proctor G, Jiang T, Iwahashi M, Wang Z, Li J, and Levi M, “Regulation of renal fatty acid and cholesterol metabolism, inflammation, and fibrosis in Akita and OVE26 mice with type 1 diabetes,” (in eng), *Diabetes*, vol. 55, no. 9, pp. 2502–9, Sep 2006, doi: 10.2337/db05-0603. [PubMed: 16936198]
- [54]. Lee JH, Phelan P, Shin M, Oh BC, Han X, Im SS, and Osborne TF, “SREBP-1a-stimulated lipid synthesis is required for macrophage phagocytosis downstream of TLR4-directed mTORC1,” (in eng), *Proc Natl Acad Sci U S A*, vol. 115, no. 52, pp. E12228–e12234, Dec 26 2018, doi: 10.1073/pnas.1813458115. [PubMed: 30530672]
- [55]. Sorrentino G et al. , “Metabolic control of YAP and TAZ by the mevalonate pathway,” *Nat Cell Biol*, vol. 16, no. 4, pp. 357–66, Apr 2014, doi: 10.1038/ncb2936. [PubMed: 24658687]
- [56]. Keller KE et al. , “Consensus recommendations for trabecular meshwork cell isolation, characterization and culture,” *Exp Eye Res*, vol. 171, pp. 164–173, Jun 2018, doi: 10.1016/j.exer.2018.03.001. [PubMed: 29526795]
- [57]. Soundararajan A, Wang T, Ghag SA, Kang MH, and Pattabiraman PP, “Novel insight into the role of clusterin on intraocular pressure regulation by modifying actin polymerization and extracellular matrix remodeling in the trabecular meshwork,” (in eng), *J Cell Physiol*, vol. 237, no. 7, pp. 3012–3029, Jul 2022, doi: 10.1002/jcp.30769. [PubMed: 35567755]
- [58]. Cheng X, Li J, and Guo D, “SCAP/SREBPs are Central Players in Lipid Metabolism and Novel Metabolic Targets in Cancer Therapy,” (in eng), *Curr Top Med Chem*, vol. 18, no. 6, pp. 484–493, 2018, doi: 10.2174/1568026618666180523104541. [PubMed: 29788888]



- [59]. Kamisuki S et al. , “A small molecule that blocks fat synthesis by inhibiting the activation of SREBP;” (in eng), *Chem Biol*, vol. 16, no. 8, pp. 882–92, Aug 28 2009, doi: 10.1016/j.chembiol.2009.07.007. [PubMed: 19716478]
- [60]. Lee SH, Lee JH, and Im SS, “The cellular function of SCAP in metabolic signaling,” (in eng), *Exp Mol Med*, vol. 52, no. 5, pp. 724–729, May 2020, doi: 10.1038/s12276-020-0430-0. [PubMed: 32385422]
- [61]. Jiajia L et al. , “Assessment of Neuronal Viability Using Fluorescein Diacetate-Propidium Iodide Double Staining in Cerebellar Granule Neuron Culture,” *J Vis Exp*, no. 123, May 10 2017, doi: 10.3791/55442.
- [62]. Kidani Y et al. , “Sterol regulatory element–binding proteins are essential for the metabolic programming of effector T cells and adaptive immunity,” *Nature Immunology*, vol. 14, no. 5, pp. 489–499, 2013/05/01 2013, doi: 10.1038/ni.2570. [PubMed: 23563690]
- [63]. Livak KJ and Schmittgen TD, “Analysis of relative gene expression data using real-time quantitative PCR and the 2(-Delta Delta C(T)) Method,” (in eng), *Methods*, vol. 25, no. 4, pp. 402–8, Dec 2001, doi: 10.1006/meth.2001.1262. [PubMed: 11846609]
- [64]. Pattabiraman PP and Rao PV, “Mechanistic basis of Rho GTPase-induced extracellular matrix synthesis in trabecular meshwork cells,” (in English), *Am J Physiol Cell Physiol*, vol. 298, no. 3, pp. C749–63, Mar 2010, doi: 10.1152/ajpcell.00317.2009. [PubMed: 19940066]
- [65]. Bligh EG and Dyer WJ, “A rapid method of total lipid extraction and purification,” (in eng), *Can J Biochem Physiol*, vol. 37, no. 8, pp. 911–7, Aug 1959, doi: 10.1139/o59-099. [PubMed: 13671378]
- [66]. Wang T and Pattabiraman PP, “Analysis of Lipid Contents in Human Trabecular Meshwork Cells by Multiple Reaction Monitoring (MRM) Profiling Lipidomics,” (in eng), *Methods Mol Biol*, vol. 2625, pp. 291–298, 2023, doi: 10.1007/978-1-0716-2966-6\_24. [PubMed: 36653651]
- [67]. Pattabiraman PP, Inoue T, and Rao PV, “Elevated intraocular pressure induces Rho GTPase mediated contractile signaling in the trabecular meshwork,” *Exp Eye Res*, vol. 136, pp. 29–33, Jul 2015, doi: 10.1016/j.exer.2015.05.001. [PubMed: 25956210]
- [68]. Zanet J, Jayo A, Plaza S, Millard T, Parsons M, and Stramer B, “Fascin promotes filopodia formation independent of its role in actin bundling,” *Journal of Cell Biology*, vol. 197, no. 4, pp. 477–486, 2012, doi: 10.1083/jcb.201110135. [PubMed: 22564415]
- [69]. Bernard O, “Lim kinases, regulators of actin dynamics,” (in eng), *Int J Biochem Cell Biol*, vol. 39, no. 6, pp. 1071–6, 2007, doi: 10.1016/j.biocel.2006.11.011. [PubMed: 17188549]
- [70]. Wu C, “Focal adhesion: a focal point in current cell biology and molecular medicine,” (in eng), *Cell Adh Migr*, vol. 1, no. 1, pp. 13–8, Jan-Mar 2007, doi: 10.4161/cam.1.1.4081. [PubMed: 19262093]
- [71]. WuDunn D, “Mechanobiology of trabecular meshwork cells,” (in eng), *Exp Eye Res*, vol. 88, no. 4, pp. 718–23, Apr 2009, doi: 10.1016/j.exer.2008.11.008. [PubMed: 19071113]
- [72]. Turner DC et al. , “Transient Intraocular Pressure Fluctuations: Source, Magnitude, Frequency, and Associated Mechanical Energy,” (in eng), *Invest Ophthalmol Vis Sci*, vol. 60, no. 7, pp. 2572–2582, Jun 3 2019, doi: 10.1167/iovs.19-26600. [PubMed: 31212310]
- [73]. Xin C, Tian N, Li M, Wang H, and Wang N, “Mechanism of the reconstruction of aqueous outflow drainage,” (in eng), *Sci China Life Sci*, vol. 61, no. 5, pp. 534–540, May 2018, doi: 10.1007/s11427-017-9140-8. [PubMed: 29282607]
- [74]. Rao PV, Pattabiraman PP, and Kopczynski C, “Role of the Rho GTPase/Rho kinase signaling pathway in pathogenesis and treatment of glaucoma: Bench to bedside research,” (in eng), *Exp Eye Res*, vol. 158, pp. 23–32, May 2017, doi: 10.1016/j.exer.2016.08.023. [PubMed: 27593914]
- [75]. Vahabikashi A et al. , “Increased stiffness and flow resistance of the inner wall of Schlemm’s canal in glaucomatous human eyes,” *Proceedings of the National Academy of Sciences*, vol. 116, no. 52, pp. 26555–26563, 2019.
- [76]. Last JA et al., “Elastic modulus determination of normal and glaucomatous human trabecular meshwork,” *Invest Ophthalmol Vis Sci*, Comparative Study Research Support, N.I.H., Extramural Research Support, Non-U.S. Gov’t vol. 52, no. 5, pp. 2147–52, Apr 2011, doi: 10.1167/iovs.10-6342. [PubMed: 21220561]

- [77]. Gao K et al. , “Reduced Pulsatile Trabecular Meshwork Motion in Eyes With Primary Open Angle Glaucoma Using Phase-Sensitive Optical Coherence Tomography,” (in eng), *Invest Ophthalmol Vis Sci*, vol. 61, no. 14, p. 21, Dec 1 2020, doi: 10.1167/iovs.61.14.21.
- [78]. Sheybani A et al. , “Open-Angle Glaucoma: Burden of Illness, Current Therapies, and the Management of Nocturnal IOP Variation,” (in eng), *Ophthalmol Ther*, vol. 9, no. 1, pp. 1–14, Mar 2020, doi: 10.1007/s40123-019-00222-z.
- [79]. Kim YM et al. , “Sterol regulatory element-binding protein (SREBP)-1-mediated lipogenesis is involved in cell senescence,” (in eng), *The Journal of biological chemistry*, vol. 285, no. 38, pp. 29069–77, Sep 17 2010, doi: 10.1074/jbc.M110.120386. [PubMed: 20615871]
- [80]. Alvarado J, Murphy C, and Juster R, “Trabecular meshwork cellularity in primary open-angle glaucoma and nonglaucomatous normals,” *Ophthalmology*, Research Support, Non-U.S. Gov’t Research Support, U.S. Gov’t, P.H.S. vol. 91, no. 6, pp. 564–79, Jun 1984. [Online]. Available: <http://www.ncbi.nlm.nih.gov/pubmed/6462622>. [PubMed: 6462622]
- [81]. Alvarado J, Murphy C, Polansky J, and Juster R, “Age-related changes in trabecular meshwork cellularity,” *Invest Ophthalmol Vis Sci*, Research Support, Non-U.S. Gov’t Research Support, U.S. Gov’t, P.H.S. vol. 21, no. 5, pp. 714–27, Nov 1981. [Online]. Available: <http://www.ncbi.nlm.nih.gov/pubmed/7298275>. [PubMed: 7298275]
- [82]. Ko F et al. , “Diabetes, Triglyceride Levels, and Other Risk Factors for Glaucoma in the National Health and Nutrition Examination Survey 2005–2008,” (in eng), *Invest Ophthalmol Vis Sci*, vol. 57, no. 4, pp. 2152–7, Apr 1 2016, doi: 10.1167/iovs.15-18373. [PubMed: 27111561]
- [83]. Sahinoglu-Keskek N, Keskek SO, Cevher S, Kirim S, Kayiklik A, Ortoglu G, and Saler T, “Metabolic syndrome as a risk factor for elevated intraocular pressure,” (in eng), *Pak J Med Sci*, vol. 30, no. 3, pp. 477–82, May 2014, doi: 10.12669/pjms.303.4514. [PubMed: 24948962]
- [84]. Chang YC, Lin JW, Wang LC, Chen HM, Hwang JJ, and Chuang LM, “Association of intraocular pressure with the metabolic syndrome and novel cardiometabolic risk factors,” (in eng), *Eye (Lond)*, vol. 24, no. 6, pp. 1037–43, Jun 2010, doi: 10.1038/eye.2009.247. [PubMed: 19816514]
- [85]. Dean JM and Lodhi IJ, “Structural and functional roles of ether lipids,” (in eng), *Protein Cell*, vol. 9, no. 2, pp. 196–206, Feb 2018, doi: 10.1007/s13238-017-0423-5. [PubMed: 28523433]
- [86]. Almsharqi ZA, “Potential Role of Plasmalogens in the Modulation of Biomembrane Morphology,” (in eng), *Front Cell Dev Biol*, vol. 9, p. 673917, 2021, doi: 10.3389/fcell.2021.673917. [PubMed: 34368127]
- [87]. Graessler J, Schwudke D, Schwarz PE, Herzog R, Shevchenko A, and Bornstein SR, “Top-down lipidomics reveals ether lipid deficiency in blood plasma of hypertensive patients,” (in eng), *PloS one*, vol. 4, no. 7, p. e6261, Jul 15 2009, doi: 10.1371/journal.pone.0006261. [PubMed: 19603071]
- [88]. Spears LD et al. , “Endothelial ether lipids link the vasculature to blood pressure, behavior, and neurodegeneration,” (in eng), *J Lipid Res*, vol. 62, p. 100079, 2021, doi: 10.1016/j.jlr.2021.100079.
- [89]. Edwards G, Aribindi K, Guerra Y, and Bhattacharya SK, “Sphingolipids and ceramides of mouse aqueous humor: Comparative profiles from normotensive and hypertensive DBA/2J mice,” *Biochimie*, vol. 105, pp. 99–109, Oct 2014, doi: 10.1016/j.biochi.2014.06.019. [PubMed: 25014247]
- [90]. Edwards G, Aribindi K, Guerra Y, Lee RK, and Bhattacharya SK, “Phospholipid profiles of control and glaucomatous human aqueous humor,” *Biochimie*, vol. 101, pp. 232–47, Jun 2014, doi: 10.1016/j.biochi.2014.01.020. [PubMed: 24561385]
- [91]. Wang H, Edwards G, Garzon C, Piqueras C, and Bhattacharya SK, “Aqueous humor phospholipids of DBA/2J and DBA/2J-Gpnmb(+)/SjJ mice,” *Biochimie*, vol. 113, pp. 59–68, Jun 2015, doi: 10.1016/j.biochi.2015.03.019. [PubMed: 25843665]
- [92]. Mettu PS, Deng PF, Misra UK, Gawdi G, Epstein DL, and Rao PV, “Role of lysophospholipid growth factors in the modulation of aqueous humor outflow facility,” *Invest Ophthalmol Vis Sci*, Research Support, Non-U.S. Gov’t Research Support, U.S. Gov’t, P.H.S. vol. 45, no. 7, pp. 2263–71, Jul 2004, doi: 10.1167/iovs.03-0960. [PubMed: 15223804]

- [93]. Ho LTY et al. , “Role of the autotaxin-lysophosphatidic acid axis in glaucoma, aqueous humor drainage and fibrogenic activity,” *Biochimica et Biophysica Acta (BBA) - Molecular Basis of Disease*, vol. 1866, no. 1, p. 165560, 2020/01/01/ 2020, doi: 10.1016/j.bbadis.2019.165560. [PubMed: 31648019]
- [94]. Honjo M et al. , “Autotaxin–Lysophosphatidic Acid Pathway in Intraocular Pressure Regulation and Glaucoma Subtypes,” *Investigative Ophthalmology & Visual Science*, vol. 59, no. 2, pp. 693–701, 2018, doi: 10.1167/iovs.17-23218. [PubMed: 29392315]
- [95]. Iyer P, Lalane R 3rd, Morris C, Challa P, Vann R, and Rao PV, “Autotaxin-lysophosphatidic acid axis is a novel molecular target for lowering intraocular pressure,” *PloS one, Research Support, American Recovery and Reinvestment Act Research Support, N.I.H., Extramural* vol. 7, no. 8, p. e42627, 2012, doi: 10.1371/journal.pone.0042627. [PubMed: 22916143]
- [96]. Lin HC, Chien CW, Hu CC, and Ho JD, “Comparison of comorbid conditions between open-angle glaucoma patients and a control cohort: a case-control study,” (in eng), *Ophthalmology*, vol. 117, no. 11, pp. 2088–95, Nov 2010, doi: 10.1016/j.ophtha.2010.03.003. [PubMed: 20570357]
- [97]. Pavljasevi S and As eri M, “Primary open-angle glaucoma and serum lipids,” (in eng), *Bosn J Basic Med Sci*, vol. 9, no. 1, pp. 85–8, Feb 2009, doi: 10.17305/bjbm.2009.2863. [PubMed: 19284402]
- [98]. Newman-Casey PA, Talwar N, Nan B, Musch DC, and Stein JD, “The relationship between components of metabolic syndrome and open-angle glaucoma,” (in eng), *Ophthalmology*, vol. 118, no. 7, pp. 1318–26, Jul 2011, doi: 10.1016/j.ophtha.2010.11.022. [PubMed: 21481477]
- [99]. Stewart WC, Sine C, Sutherland S, and Stewart JA, “Total cholesterol and high-density lipoprotein levels as risk factors for increased intraocular pressure,” (in eng), *Am J Ophthalmol*, vol. 122, no. 4, pp. 575–7, Oct 1996, doi: 10.1016/s0002-9394(14)72121-x. [PubMed: 8862057]
- [100]. McCann P, Hogg RE, Fallis R, and Azuara-Blanco A, “The Effect of Statins on Intraocular Pressure and on the Incidence and Progression of Glaucoma: A Systematic Review and Meta-Analysis,” *Investigative Ophthalmology & Visual Science*, vol. 57, no. 6, pp. 2729–2748, 2016, doi: 10.1167/iovs.15-18595. [PubMed: 27196321]
- [101]. Talwar N, Musch DC, and Stein JD, “Association of Daily Dosage and Type of Statin Agent With Risk of Open-Angle Glaucoma,” (in eng), *JAMA ophthalmology*, vol. 135, no. 3, pp. 263–267, Mar 1 2017, doi: 10.1001/jamaophthalmol.2016.5406. [PubMed: 28114645]
- [102]. Song XY, Chen YY, Liu WT, Cong L, Zhang JL, Zhang Y, and Zhang YY, “Atorvastatin reduces IOP in ocular hypertension in vivo and suppresses ECM in trabecular meshwork perhaps via FGD4,” (in eng), *Int J Mol Med*, vol. 49, no. 6, Jun 2022, doi: 10.3892/ijmm.2022.5132.
- [103]. Cong L, Fu S, Zhang J, Zhao J, and Zhang Y, “Effects of atorvastatin on porcine aqueous humour outflow and trabecular meshwork cells,” (in eng), *Exp Ther Med*, vol. 15, no. 1, pp. 210–216, Jan 2018, doi: 10.3892/etm.2017.5353. [PubMed: 29250149]
- [104]. Von Zee CL and Stubbs EB Jr., “Geranylgeranylation facilitates proteasomal degradation of rho G-proteins in human trabecular meshwork cells,” *Invest Ophthalmol Vis Sci*, vol. 52, no. 3, pp. 1676–83, Mar 2011, doi: 10.1167/iovs.10-6171. [PubMed: 21212187]
- [105]. Lakk M et al. , “Membrane cholesterol regulates TRPV4 function, cytoskeletal expression, and the cellular response to tension,” (in eng), *Journal of lipid research*, vol. 62, pp. 100145–100145, 2021, doi: 10.1016/j.jlr.2021.100145. [PubMed: 34710431]
- [106]. Yang YF, Sun YY, Peters DM, and Keller KE, “The Effects of Mechanical Stretch on Integrins and Filopodial-Associated Proteins in Normal and Glaucomatous Trabecular Meshwork Cells,” (in eng), *Front Cell Dev Biol*, vol. 10, p. 886706, 2022, doi: 10.3389/fcell.2022.886706. [PubMed: 35573666]
- [107]. Humphries JD, Wang P, Streuli C, Geiger B, Humphries MJ, and Ballestrem C, “Vinculin controls focal adhesion formation by direct interactions with talin and actin,” (in eng), *The Journal of cell biology*, vol. 179, no. 5, pp. 1043–57, Dec 3 2007, doi: 10.1083/jcb.200703036. [PubMed: 18056416]
- [108]. Reinhard M, Rüdiger M, Jockusch BM, and Walter U, “VASP interaction with vinculin: a recurring theme of interactions with proline-rich motifs,” (in eng), *FEBS Lett*, vol. 399, no. 1–2, pp. 103–7, Dec 9 1996, doi: 10.1016/s0014-5793(96)01295-1. [PubMed: 8980130]

- [109]. Bellis SL, Miller JT, and Turner CE, “Characterization of tyrosine phosphorylation of paxillin in vitro by focal adhesion kinase,” (in eng), *The Journal of biological chemistry*, vol. 270, no. 29, pp. 17437–41, Jul 21 1995, doi: 10.1074/jbc.270.29.17437. [PubMed: 7615549]
- [110]. López-Colomé AM, Lee-Rivera I, Benavides-Hidalgo R, and López E, “Paxillin: a crossroad in pathological cell migration,” (in eng), *J Hematol Oncol*, vol. 10, no. 1, p. 50, Feb 18 2017, doi: 10.1186/s13045-017-0418-y. [PubMed: 28214467]
- [111]. Machesky LM and Li A, “Fascin: Invasive filopodia promoting metastasis,” (in eng), *Commun Integr Biol*, vol. 3, no. 3, pp. 263–270, 2010, doi: 10.4161/cib.3.3.11556. [PubMed: 20714410]
- [112]. Jaiswal R, Breitsprecher D, Collins A, Corrêa Ivan R., Xu M-Q, and Goode Bruce L., “The Formin Daam1 and Fascin Directly Collaborate to Promote Filopodia Formation,” *Current Biology*, vol. 23, no. 14, pp. 1373–1379, 2013/07/22/ 2013, doi: 10.1016/j.cub.2013.06.013. [PubMed: 23850281]
- [113]. Vignjevic D , Kojima S.-i. , Aratyn Y , Danciu O , Svitkina T , and Borisy GG “Role of fascin in filopodial protrusion,” *Journal of Cell Biology*, vol. 174, no. 6, pp. 863–875, 2006, doi: 10.1083/jcb.200603013. [PubMed: 16966425]
- [114]. Morales-Quinones M et al. , “LIMK (LIM Kinase) Inhibition Prevents Vasoconstriction- and Hypertension-Induced Arterial Stiffening and Remodeling,” (in eng), *Hypertension*, vol. 76, no. 2, pp. 393–403, Aug 2020, doi: 10.1161/hypertensionaha.120.15203. [PubMed: 32594801]
- [115]. Geiger B, Bershadsky A, Pankov R, and Yamada KM, “Transmembrane crosstalk between the extracellular matrix--cytoskeleton crosstalk,” (in eng), *Nat Rev Mol Cell Biol*, vol. 2, no. 11, pp. 793–805, Nov 2001, doi: 10.1038/35099066. [PubMed: 11715046]
- [116]. Sotodosos-Alonso L, Pulgarín-Alfaro M, and del Pozo MA, “Caveolae Mechanotransduction at the Interface between Cytoskeleton and Extracellular Matrix,” *Cells*, vol. 12, no. 6, p. 942, 2023. [Online]. Available: <https://www.mdpi.com/2073-4409/12/6/942>. [PubMed: 36980283]
- [117]. Elliott MH et al. , “Caveolin-1 modulates intraocular pressure: implications for caveolae mechanoprotection in glaucoma,” *Scientific Reports*, vol. 6, no. 1, p. 37127, 2016/11/14 2016, doi: 10.1038/srep37127. [PubMed: 27841369]
- [118]. Golani G, Ariotti N, Parton RG, and Kozlov MM, “Membrane Curvature and Tension Control the Formation and Collapse of Caveolar Superstructures,” *Developmental Cell*, vol. 48, no. 4, pp. 523–538.e4, 2019/02/25/ 2019, doi: 10.1016/j.devcel.2018.12.005. [PubMed: 30661987]
- [119]. Jung MY et al. , “Fatty acid synthase is required for profibrotic TGF-beta signaling,” *FASEB J*, vol. 32, no. 7, pp. 3803–3815, Jul 2018, doi: 10.1096/fj.201701187R. [PubMed: 29475397]
- [120]. Lee M, Katerelos M, Gleich K, Galic S, Kemp BE, Mount PF, and Power DA, “Phosphorylation of Acetyl-CoA Carboxylase by AMPK Reduces Renal Fibrosis and Is Essential for the Anti-Fibrotic Effect of Metformin,” *J Am Soc Nephrol*, vol. 29, no. 9, pp. 2326–2336, Sep 2018, doi: 10.1681/ASN.2018010050. [PubMed: 29976587]
- [121]. Bates J et al. , “Acetyl-CoA carboxylase inhibition disrupts metabolic reprogramming during hepatic stellate cell activation,” *J Hepatol*, vol. 73, no. 4, pp. 896–905, Oct 2020, doi: 10.1016/j.jhep.2020.04.037. [PubMed: 32376414]
- [122]. Lin S-N et al. , “Development of antifibrotic therapy for stricturing Crohn’s disease: lessons from randomized trials in other fibrotic diseases,” *Physiological Reviews*, vol. 102, no. 2, pp. 605–652, 2022, doi: 10.1152/physrev.00005.2021. [PubMed: 34569264]
- [123]. Martin M et al. , “Role of endothelial cells in pulmonary fibrosis via SREBP2 activation,” (in eng), *JCI Insight*, vol. 6, no. 22, Nov 22 2021, doi: 10.1172/jci.insight.125635.
- [124]. Matsumoto M et al. , “Acetyl-CoA carboxylase 1 and 2 inhibition ameliorates steatosis and hepatic fibrosis in a MC4R knockout murine model of nonalcoholic steatohepatitis,” (in eng), *PloS one*, vol. 15, no. 1, pp. e0228212–e0228212, 2020, doi: 10.1371/journal.pone.0228212. [PubMed: 31990961]
- [125]. Bailey JNC et al. , “Hypothesis-independent pathway analysis implicates GABA and Acetyl-CoA metabolism in primary open-angle glaucoma and normal-pressure glaucoma,” *Hum Genet*, vol. 133, no. 10, pp. 1319–1330, 2014/10/01 2014, doi: 10.1007/s00439-014-1468-7. [PubMed: 25037249]

- [126]. Uttarwar L, Gao B, Ingram AJ, and Krepinsky JC, "SREBP-1 activation by glucose mediates TGF- $\beta$  upregulation in mesangial cells," (in eng), *Am J Physiol Renal Physiol*, vol. 302, no. 3, pp. F329–41, Feb 1 2012, doi: 10.1152/ajprenal.00136.2011. [PubMed: 22031849]
- [127]. Ferrari A, Maretto S, Girotto D, Volpin D, and Bressan GM, "SREBP contributes to induction of collagen VI transcription by serum starvation," *Biochem Biophys Res Commun*, vol. 313, no. 3, pp. 600–5, Jan 16 2004, doi: 10.1016/j.bbrc.2003.11.159. [PubMed: 14697233]
- [128]. Van Krieken R et al. , "Sterol Regulatory Element Binding Protein (SREBP)-1 is a novel regulator of the Transforming Growth Factor (TGF)- $\beta$  receptor I (T $\beta$ RI) through exosomal secretion," (in eng), *Cell Signal*, vol. 29, pp. 158–167, Jan 2017, doi: 10.1016/j.cellsig.2016.11.004. [PubMed: 27826032]

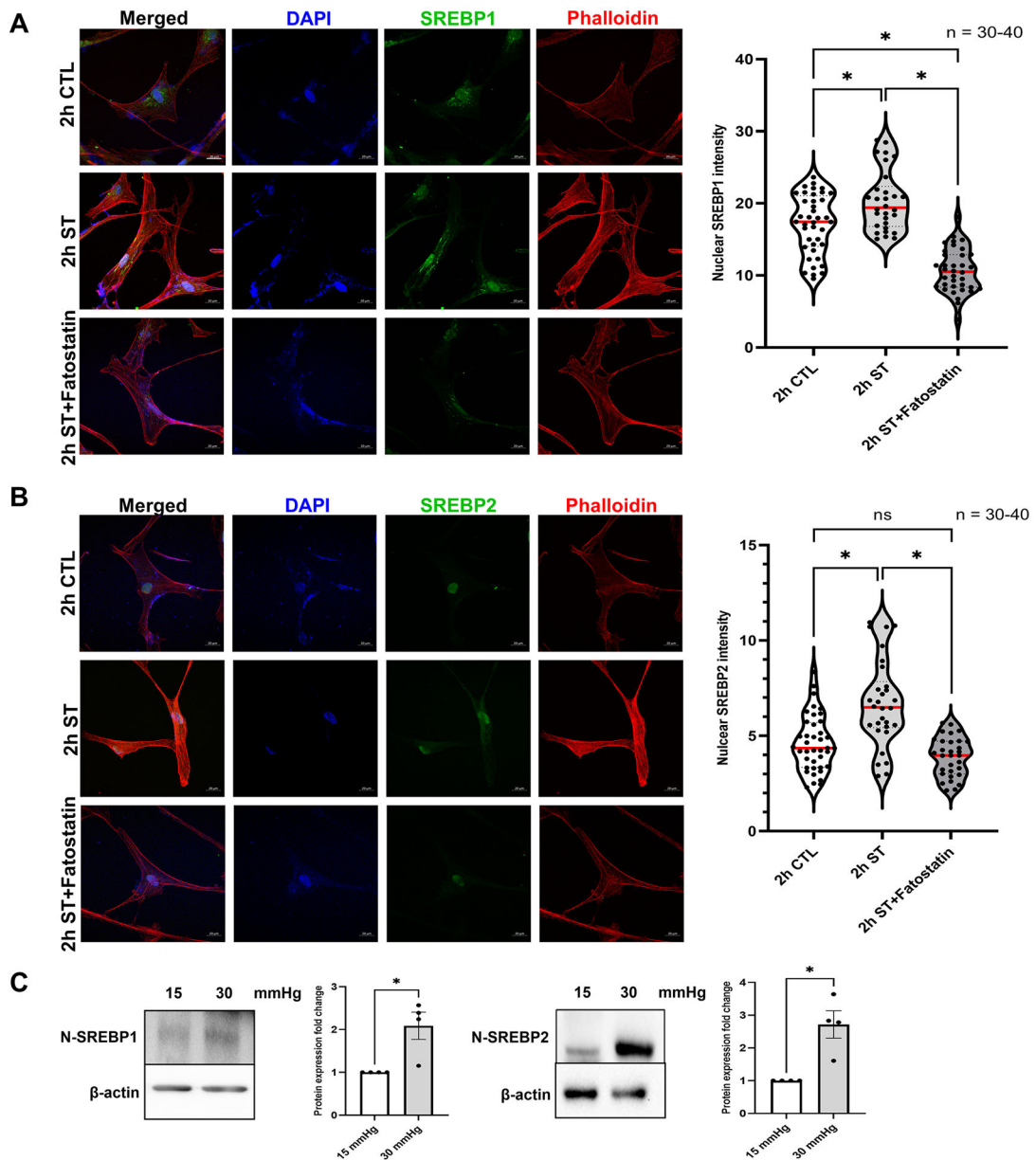


**Fig. 1: Mechanical stress on trabecular meshwork induces SREBPs activation.**

(A) and (B) Localization of SREBPs in HTM cells subjected to cyclic mechanical stretch was checked using immunofluorescence (IF). After 2 h of mechanical stress, HTM cells show a strong nuclear localization of both SREBP1 and SREBP2 (second-row third column). Phalloidin was used to stain the distribution of filamentous actin (F-actin) fiber in the cells. After 2 h of mechanical stress, there was increased F-actin distribution inside the HTM cells (second-row fourth column). 2 h stretch combined with fatostatin treatment shows decreased nuclear localization of both SREBP1 and SREBP2 (third-row third column) and decreased F-actin distribution inside the HTM cells (third-row fourth column). Quantification of immunofluorescence images using ImageJ-based fluorescence intensity measurements shows a significant increase in both nuclear SREBP1 and nuclear

SREBP2 mean fluorescence intensity in 2 h stretched HTM cells and a significant decrease in 2 h stretch combined with fatostatin treatment (right panel). The nucleus was stained with DAPI in blue. Images were captured in z-stack in a confocal microscope, and stacks were orthogonally projected. Scale bar 20 micron. (C) Protein expression of both nuclear form SREBP1 (N-SREBP1) and SREBP2 (N-SREBP2) was significantly increased in TM derived from enucleated porcine anterior segments perfused under the elevated pressure of 30 mmHg for 5 h compared with 15 mmHg. The results were based on semi-quantitative immunoblotting with subsequent densitometric analysis.  $\beta$ -actin was used as a loading control. Values represent the mean  $\pm$  SEM, where n = 4–40 (including biological replicates and experimental replicates). \*p < 0.05 was considered statistically significant. CTL: un-stretched control HTM cells, ST: stretched HTM cells.

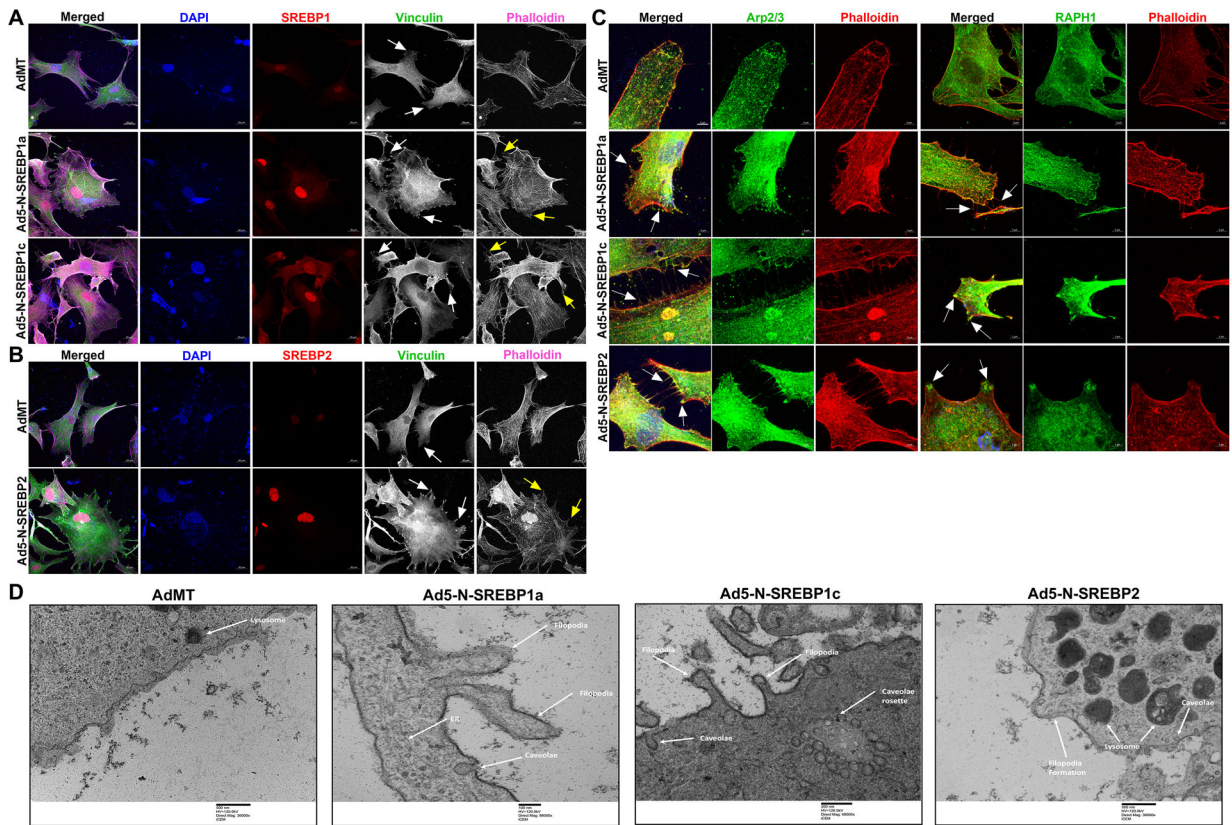


**Fig. 2: Constitutive induction of SREBPs activation modulates actin and focal adhesion dynamics.**

(A) and (B) Immunofluorescence (IF) shows the distribution of SREBP1, SREBP2, filamentous actin (F-actin) fibers, and vinculin in HTM cells under AdMT and Ad5-N-SREBPs treatments. (A) Ad5-N-SREBP1a (second-row third column), and Ad5-N-SREBP1c (third-row third column) induced strong staining of SREBP1 in the nucleus in HTM cells compared to AdMT (first-row third column). Similarly, (B) Ad5-N-SREBP2 (second-row third column) induced strong staining of SREBP2 in the nucleus in HTM cells compared to AdMT (first-row third column). Compared to AdMT (first-row fifth column), (A) Ad5-N-SREBP1a (second-row fifth column) and Ad5-N-SREBP1c (third-row fifth column), and (B) Ad5-N-SREBP2 (second-row fifth column) caused the increased distribution of F-actin fibers stained by phalloidin (purple/grayscale) in HTM cells and induced increased lamellipodia and filopodia formation (indicated by yellow arrows). (A) Ad5-N-SREBP1a (second-row fourth column), Ad5-N-SREBP1c (third-row fourth column), and (B) Ad5-N-SREBP2 (second-row fourth column) also induced more distribution of vinculin (green/grayscale) at the edges of F-actin fibers (indicated by white arrows) in HTM cells compared to the AdMT (first-row fourth column). The nucleus was stained with DAPI in blue. Images were captured in z-stack in a confocal microscope, and stacks were orthogonally projected. Scale bar 20 micron. (C) Immunofluorescence (IF) shows the distribution of Arp2/3 and RAPH1 in HTM cells under AdMT and Ad5-N-SREBPs treatment. Compared to AdMT, Ad5-N-SREBPs induced the distribution of Arp2/3 and RAPH1 at the cell membrane and near the filopodia structures. Images were captured in



z-stack in a confocal microscope, and stacks were orthogonally projected. Scale bar 5 micron. **(D)** Transmission electron microscope (TEM) image of HTM cells under AdMT and Ad5-N-SREBPs treatment. Compared to AdMT, Ad5-N-SREBP1a, Ad5-N-SREBP1c, and Ad5-N-SREBP2 induced membrane bending and filopodia formation. Scale bar as shown in the figure.

Author Manuscript

Author Manuscript

Author Manuscript

Author Manuscript

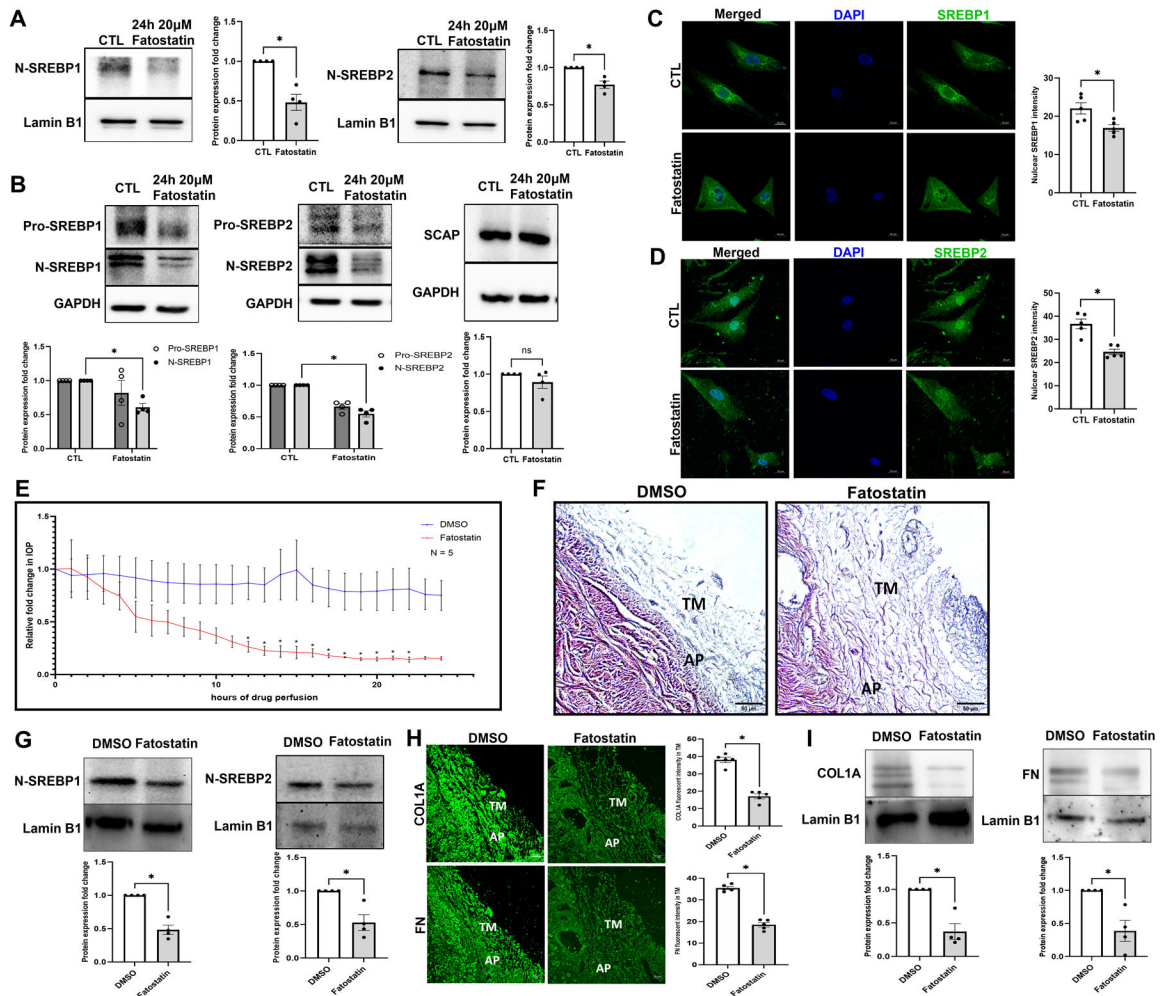


**Fig. 3: Pharmacological inhibition of SCAP-SREBP pathway lowers IOP.**

(A) Nuclear fraction from PTM cells after 20  $\mu$ M fatostatin for 24 h treatment.

Immunoblotting result shows that both N-SREBP1 (left panel) and N-SREBP2 (right panel) were significantly decreased. Lamin B1 was used as a loading control. (B)

Primary HTM cells were treated with 20  $\mu$ M fatostatin for 24 h, and immunoblotting results show that both N-SREBP1 (left panel) and N-SREBP2 (middle panel) were significantly decreased under fatostatin treatment, but SCAP protein expression level was not significantly different in two groups (right panel). GAPDH was used as a loading control. (C) and (D) Immunofluorescence (IF) shows the changes in SREBP1 and SREBP2

distribution in HTM cells after 20  $\mu$ M fatostatin treatment (left panel). In the fatostatin treated HTM cells, less SREBP1 (green staining) and SREBP2 (green staining) were distributed inside the nucleus (second row), compared to DMSO treated control HTM cells (first row). The nucleus was stained with DAPI in blue. Images were captured in z-stack in a confocal microscope, and stacks were orthogonally projected. Scale bar 20 microns. Quantification of immunofluorescence images using ImageJ-based fluorescence intensity measurements shows a significant decrease in both nuclear SREBP1 and nuclear SREBP2 mean fluorescence intensity in fatostatin treated HTM cells (right panel). Freshly enucleated porcine eyes were perfused with 20  $\mu$ M fatostatin or DMSO control after

baseline was established with perfusion media containing D-glucose at 37 °C. **(E)** Graphical representation of relative fold change in IOP showed a significant decrease post 12 h of fatostatin perfusion (red line) and remained significant until 22 h compared to vehicle DMSO perfused control (blue line). **(F)** Histological examination of the outflow pathway tissues using Hematoxylin and Eosin (H and E) staining showed increased spacing between the TM in the fatostatin perfused eyes compared to a more compact TM in the DMSO perfused eyes. Scale bar 50 micron. **(G)** Quantitative analysis of protein expression from 20  $\mu$ M fatostatin perfused TM tissues showed a significant decrease in N-SREBP1 and N-SREBP2, compared to vehicle DMSO perfused control. Lamin B1 was used as a loading control. **(H)** Immunolocalization of ECM proteins, including COL1A and FN (green staining) in the outflow pathway tissue in DMSO control or fatostatin. In the fatostatin perfused eyes, COL1A and FN (left panel second column) showed a decreased distribution in the TM-JCT region. TM indicates trabecular meshwork. AP indicates aqueous plexus. Images were captured in z-stack in a confocal microscope, and stacks were orthogonally projected. Scale bar 50 micron. Quantification of immunofluorescence images using ImageJ-based fluorescence intensity measurements showed a significant decrease in the fluorescence intensity of COL1A and FN in the TM outflow pathway (right panel). **(I)** Quantitative analysis of protein expression from 20  $\mu$ M fatostatin perfused TM tissues showed a significant decrease in COL1A, and FN compared to vehicle DMSO perfused control. Lamin B1 was used as a loading control. Values represent the mean  $\pm$  SEM, where n = 4–5 (biological replicates). \*p < 0.05 was considered statistically significant.

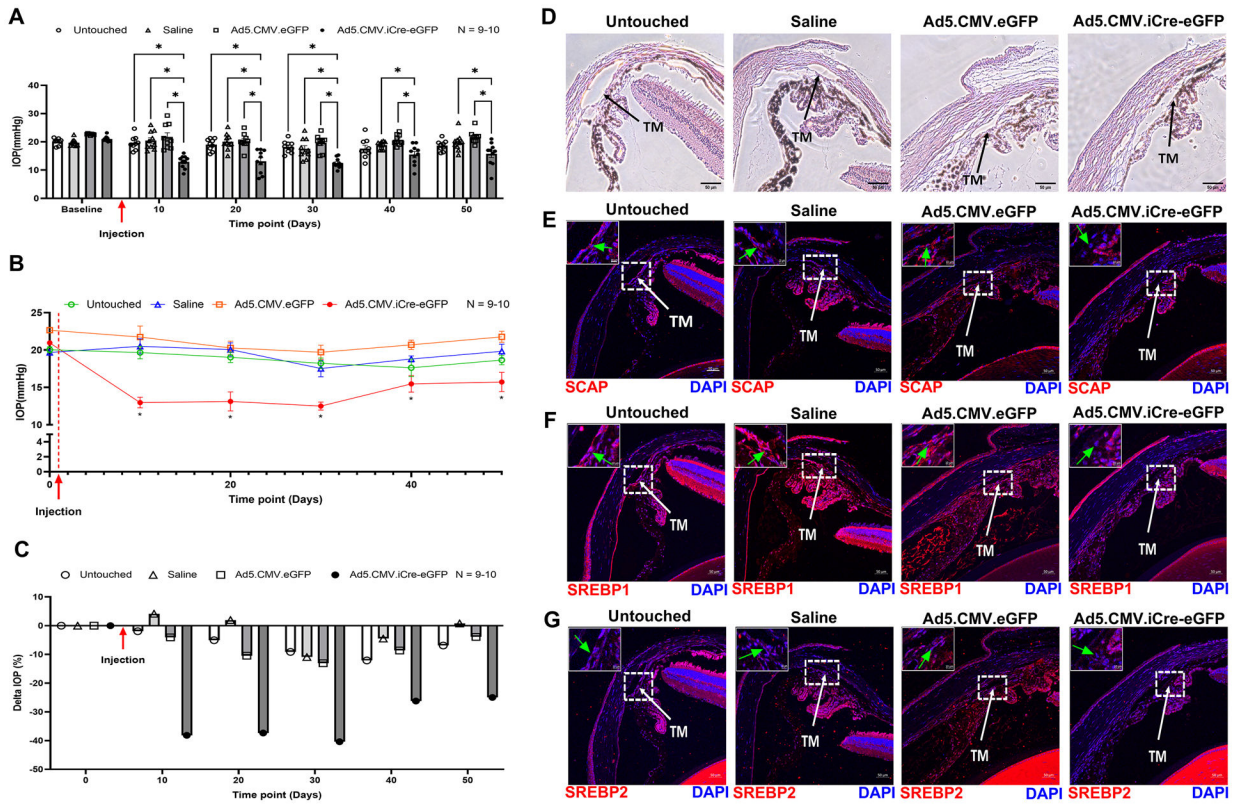


**Fig. 4: Molecular inactivation of SREBPs by SCAP knockdown lowers IOP**

(A) Starting from 10 days after saline and adenovirus injection, IOP was significantly decreased in Ad5.CMV.iCre-eGFP injection group compared to the untouched group, saline injection group, and Ad5.CMV.eGFP injection group. This significant reduction in IOP in Ad5.CMV.iCre-eGFP injection group was sustained until 30 days post-injection. On 40 days and 50 days post-injection, compared to saline injection group and Ad5.CMV.eGFP injection group, IOP in Ad5.CMV.iCre-eGFP injection group was significantly decreased, it was also lower than the untouched group, but not statistically significant. (B) IOP changes in each group were analyzed and compared to their baseline normal IOP (before injection/time point 0 days), the graphical representation shows that IOP was significantly decreased in Ad5.CMV.iCre-eGFP injection group starting from 10 days after injection and sustained until 50 days post-injection. There were no significant changes in IOP levels in other control groups. (C) IOP percentage change (Delta IOP) compared to their baseline normal IOP in each group was calculated, and a graphical representation shows that IOP in Ad5.CMV.iCre-eGFP injection group was decreased as much as 40.38 % of baseline normal (before injection/time point 0 days) with an average decrease of 27.85 %. The IOP in other control groups showed less than 13 % changes of baseline normal IOP. (D) Histological examination of the TM using Hematoxylin and Eosin (H and E) staining showed no gross morphological alterations between four groups. Scale bar 50 micron. (E), (F) and (G) Immunolocalization of SCAP, SREBP1 and SREBP2 proteins in TM in four groups. SCAP showed decreased distribution in TM in Ad5.CMV.iCre-eGFP injection group compared to all other sham control groups. SREBP1 and SREBP2 showed decreased distribution in the nuclear regions in TM in Ad5.CMV.iCre-eGFP injection group compared to other sham

control groups. TM indicates trabecular meshwork and marked by white color arrow. Images were captured in z-stack in a confocal microscope, and stacks were orthogonally projected. Scale bar 50 micron. The top left corner in each image shows the magnification of the framed area showing the nuclear regions in TM and marked by green color arrow. Scale bar 10 micron. Values represent the mean  $\pm$  SEM, where n = 9–10 (biological replicates). \*p < 0.05 was considered statistically significant.

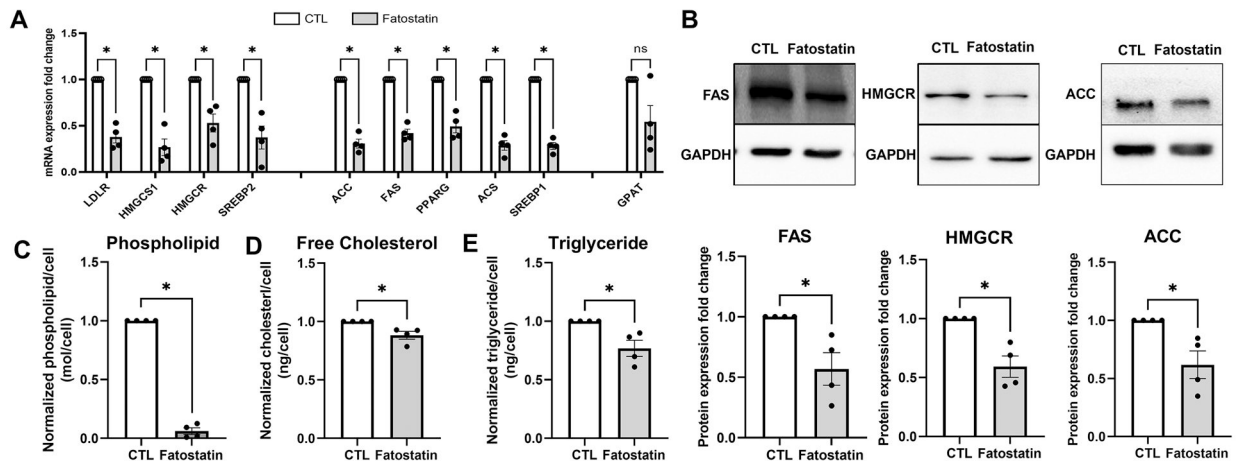


**Fig. 5: Inactivation of SREBPs inhibits lipogenesis in HTM cells.**

(A) Fatostatin treatment significantly decreased SREBPs responsive genes mRNA expression involved in 1) cholesterol biosynthesis: low-density lipoprotein receptor (LDLR), hydroxymethylglutaryl-CoA synthase 1 (HMGCS1), 3-hydroxy-3-methylglutaryl-CoA Reductase (HMGCR), SREBP2; 2) fatty acid biosynthesis: acetyl-CoA carboxylase (ACC), fatty acid synthase (FAS), SREBP1, peroxisome proliferator- activated receptor gamma (PPARG), acetyl-CoA synthetase (ACS); 3) triglyceride and phospholipid biosynthesis: glycerol-3-phosphate acyltransferase (GPAT). 18S were used as internal controls for qPCR analysis. (B) Immunoblotting shows that fatostatin significantly reduced FAS, HMGCR, and ACC protein expression compared to the control. GAPDH was used as loading control. (C), (D) and (E) show that fatostatin significantly reduced total lipid biosynthesis in HTM cells, including normalized phospholipid/cell, normalized cholesterol/cell, and normalized triglyceride/cell. Values represent the mean  $\pm$  SEM, where n = 4 (biological replicates). \*p < 0.05 was considered statistically significant.

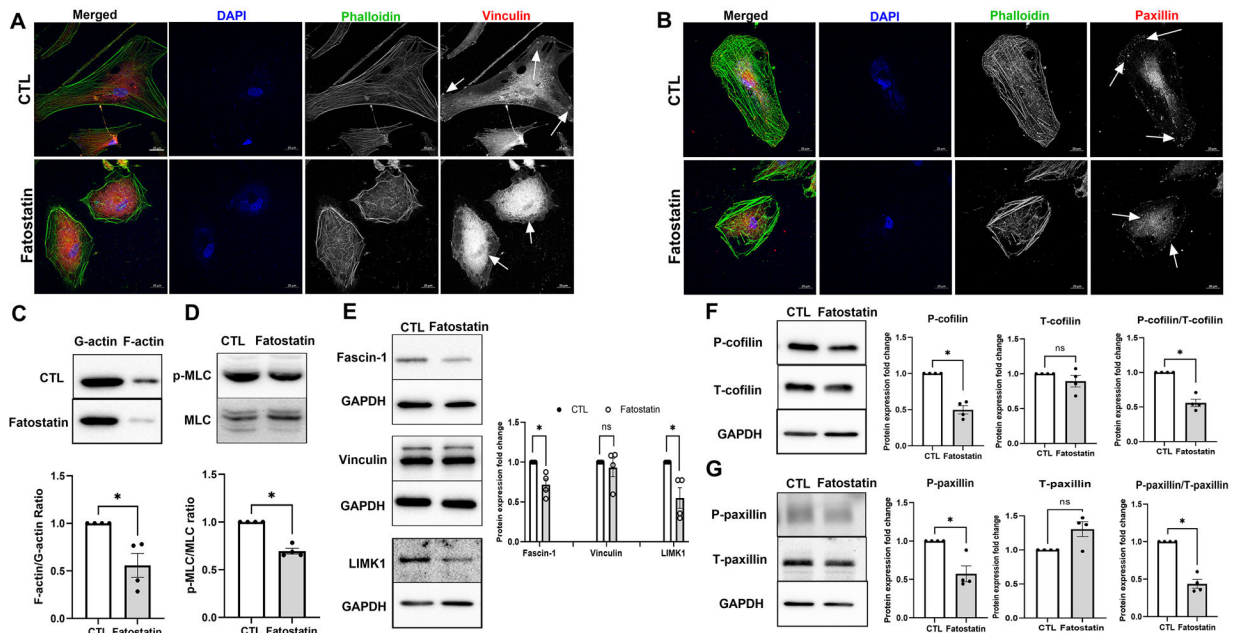


**Fig. 6: SREBPs inactivation hampers actin polymerization machinery and disengages focal adhesions.**

(A) and (B) Immunofluorescence (IF) shows the distribution of filamentous actin (F-actin) fiber, vinculin, and paxillin distribution in HTM cells under DMSO and fatostatatin treatment. Fatostatatin caused the reduced distribution of F-actin fiber stained by phalloidin (green/grayscale) in HTM cells (first and third column) compared to the control. Fatostatatin treatment resulted in less distribution of vinculin (red/grayscale) and paxillin (red/grayscale) at the edges of F-actin fiber, but more cytoplasmic distribution (indicated by white arrows) in HTM cells (first and fourth column) compared to the control. The nucleus was stained with DAPI in blue. Images were captured in z-stack in a confocal microscope, and stacks were orthogonally projected. Scale bar 20 micron. (C) Globular actin (G-actin) and F-actin were extracted from HTM cells treated with DMSO or fatostatatin. Immunoblotting shows that fatostatatin significantly decreased F-actin/G-actin ratio in HTM cells compared to the control. (D) Immunoblotting shows that fatostatatin treatment significantly decreased p-MLC/MLC ratio in HTM cells. (E) Immunoblotting shows that fatostatatin treatment significantly reduced Fascin-1 and LIMK1 protein expression, but no difference in vinculin expression compared to the control. GAPDH was used as a loading control. (F) Immunoblotting shows that there was no significant difference in total-cofilin (T-cofilin) protein expression levels in DMSO and fatostatatin treated HTM cells. The phospho-cofilin (P-cofilin) and the ratio of P-cofilin/T-cofilin were significantly decreased in fatostatatin treated HTM cells compared to the control. GAPDH was used as a loading control. (G) Immunoblotting shows that fatostatatin significantly decreased phospho-paxillin (P-paxillin) protein expression level, increased total-paxillin (T-paxillin) protein expression level, and significantly reduced the ratio of P-paxillin/T-paxillin compared to the control. GAPDH was used as a loading control. Values represent the mean  $\pm$  SEM, where  $n = 4$  (biological replicates). \* $p < 0.05$  was considered statistically significant, and ns denotes non-significant.

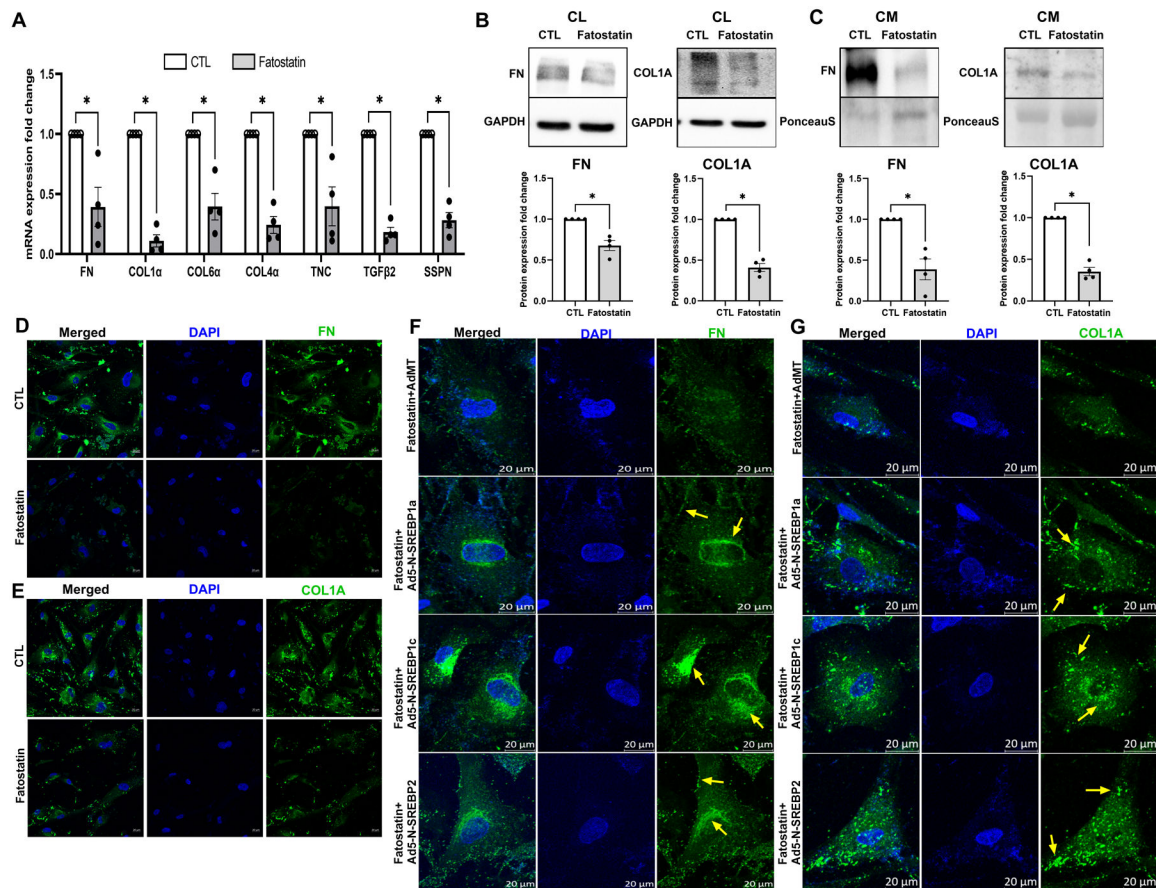


**Fig. 7: SREBP activation is a critical regulator of ECM engagement to the matrix sites.** (A) Regulation of ECM mRNA expression under fatostatin treatment. Fatostatin treatment significantly decreased mRNA expression in fibronectin (FN), collagen 1 (COL1), collagen 6 (COL6), collagen 4 (COL4), tenascin C (TNC), transforming growth factor  $\beta$  2 (TGF $\beta$ 2), and sarcospan (SSPN) in HTM cells compared to DMSO treated control HTM cells. (B) Immunoblotting for whole cell lysate (CL) shows that fatostatin significantly decreased FN, and COL1A protein expression compared to DMSO treated control HTM cells. GAPDH was used as a loading control. (C) Immunoblotting for conditioned media (CM) shows that fatostatin significantly decreased FN and COL1A protein expression in HTM CM compared to DMSO treated control HTM CM. Ponceau S was used as a loading control. (D) and (E) Immunofluorescence (IF) shows the FN and COL1A expression and distribution in HTM cells after DMSO or fatostatin treatment. Fatostatin reduced FN (green staining) and COL1A (green staining) distribution compared to the control. The nucleus was stained with DAPI in blue. (F) and (G) Immunofluorescence (IF) shows that compared to fatostatin combined with AdMT treatment (first-row third column), there was increased FN and COL1A expression and distribution in HTM cells in fatostatin combined with Ad5-N-SREBP1a (second-row third column), Ad5-N-SREBP1c (third-row third column) and Ad5-N-SREBP2 (fourth-row third column) treatments. The nucleus was stained with DAPI in blue. Images were captured in z-stack in a confocal microscope, and stacks were orthogonally projected. Scale bar 20 micron. The lower magnification images of the cells



can be visualized in the Supplementary Figure 7. Values represent the mean  $\pm$  SEM, where n = 4 (biological replicates). \*p < 0.05 was considered statistically significant.

Author Manuscript

Author Manuscript

Author Manuscript

Author Manuscript

**TABLE 1:**

## Antibodies and Reagents:

Reagents and antibodies	Catalog number	Company
Vinculin	V9131	Millipore Sigma
$\beta$ -actin	A1798	Millipore Sigma
Collagen 1a (COL1A)	ab34710	Abcam
RAPH1	PA5-110270	Invitrogen/ThermoFisher
Arp2/3	07-227-1	Sigma-Aldrich
LIMK1	sc515585	Santa Cruz Biotechnology
SREBP1	sc13551	Santa Cruz Biotechnology
SREBP2	sc13552	Santa Cruz Biotechnology
Paxillin	sc365379	Santa Cruz Biotechnology
GAPDH	sc32233	Santa Cruz Biotechnology
FAS	sc-48357	Santa Cruz Biotechnology
Fascin 1	sc46675	Santa Cruz Biotechnology
SREBP1	NB100-2215	NOVUS Biologicals
SREBP2	NBP1-54446	NOVUS Biologicals
SREBP2	LS-B1609-BCD1-1	Life Span Bioscience
SCAP	12266-1-AP	Proteintech
SCAP	MABS2288	Sigma-Aldrich
Collagen 1a (COL1A)	ABT257	Sigma-Aldrich
HMGCR	PA5-37367	Invitrogen/ThermoFisher
Lamin B1	PA5-19468	Invitrogen/ThermoFisher
Total-paxillin (T-paxillin)	2542S	Cell Signaling Technology
Phospho-paxillin (P-paxillin)	69363S	Cell Signaling Technology
Total-cofilin (T-cofilin)	5175S	Cell Signaling Technology
Phospho-cofilin (P-cofilin)	3311S	Cell Signaling Technology
Phospho-myosin light chain (p-MLC)	3671	Cell Signaling Technology
Myosin light chain (MLC)	3672	Cell Signaling Technology
ACC	3662S	Cell Signaling Technology
Fibronectin		Gift from Dr. Harold Erickson, Duke University
Donkey-anti-goat IgG	705-035-003	Jackson ImmunoResearch
Donkey-anti-mouse IgG	715-035-150	Jackson ImmunoResearch
Donkey-anti-rabbit IgG	715-035-144	Jackson ImmunoResearch
Goat-anti-Mouse IgG Alexa Fluro Plus 488	A32723	ThermoFisher
Goat-anti-Mouse IgG Alexa Fluor Plus 594	A32742	ThermoFisher
Goat-anti-Rabbit IgG Alexa Fluor Plus 488	A32731	ThermoFisher
Goat-anti-Rabbit IgG Alexa Fluor Plus 594	A32740	ThermoFisher
Phalloidin (Alexa Fluor Plus 488 PHA)	A12379	Invitrogen/ThermoFisher
Phalloidin (Alexa Fluor Plus 647 PHA)	A22287	Invitrogen/ThermoFisher

Reagents and antibodies	Catalog number	Company
DAPI	UH2820551	Sigma-Aldrich
Fluoromount-G	E139999	Invitrogen/ThermoFisher
Fatostatin	341329	Sigma-Aldrich

Author Manuscript

Author Manuscript

Author Manuscript

Author Manuscript

**TABLE 2:**

Oligonucleotides used for qPCR:

SREBP1 Transcript 1 (F1V1)	Forward	CTGACCGACATCGAAGGTGA
	Reverse	AAGTGCAATCCATGGCTCCG
SREBP1 Transcript 2 (F1V2)	Forward	GCTGACCGACATCGAAGACA
	Reverse	CAGGAGGTGGAGACAAGCTG
SREBP1 Transcript 3 (F1V3)	Forward	AACGGCTTCAAAAATCCGCC
	Reverse	CCAGCATAGGGTGGGTCAA
SREBP2 Transcript 1 (F2V1)	Forward	GGTTGTCGGGTGTCATGGG
	Reverse	TTGCAGCATCTCGTCGATGT
SCAP Transcript 1	Forward	CTGGAGAAGCTGGACTGAGC
	Reverse	CCCAAAGTGCCTGACAGATG
Total-SREBP1	Forward	CAACACAGCAACCAGAAACTC
	Reverse	CTCCACCTCAGTCTTCACG
Total-SREBP2	Forward	ATTCAGCACCACTCCGCAG
	Reverse	GCCCCATCATTACAGCATTG
LDLR	Forward	TTCACTCCATCTCAAGCATCG
	Reverse	ACTGAAAATGGCTTCGTTGATG
HMGCS1	Forward	TTCCCTTGCATCTGTTCTAGC
	Reverse	TTTTATCAAGAGCAGACCCCG
HMGCR	Forward	ACAGATACTTGGGAATGCAGAG
	Reverse	CTGTCGGCGAATAGATACACC
ACC	Forward	ACAGTGGAGCAAGAATCGG
	Reverse	AATGGACAGAGTTGAGAGCAC
FAS	Forward	AAGCTCTTCACTTCGGAGG
	Reverse	GGGCATTAACACTTTTGGACG
PPARG	Forward	ATCAAAGTGGAGCCTGCATC
	Reverse	CGACATTCAATTGCCATGAG
ACS	Forward	GGGAAGAGTTGGAAGGTGAAG
	Reverse	GCAGCCATCTCCTGTAACATAG
GPAT	Forward	GTGGAGTGTAGCAAGAGGTG
	Reverse	CAGGGAAAGTAGAGCAGACAC
FN	Forward	GGTGACACTTATGAGCGTCCTAAA
	Reverse	AACATGTAACCACAGTCTCATGTG
COL1a	Forward	GAGAGCATGACCGATGGATT
	Reverse	CCTTCTTGAGGTTGCCAGTC
COL4a	Forward	TGTGGATCGGCTACTCTTTTG
	Reverse	TAGTAATTGCAGGTCCCACG
COL6a	Forward	TCAAAGTCCTTCAACCAAGCG
	Reverse	ATCTCCACCTCGTCACTGTA

TNC	Forward	CACTACACAGCCAAGATCCAG
	Reverse	TCGTGTCTCCATTCAGCATTG
TGF $\beta$ 2	Forward	TTGACGTCTCAGCAATGGAG
	Reverse	TTCGCCTTCTGCTCTTGTTT
SSPN	Forward	AGGTTGACGAACGGACATG
	Reverse	TGTGAGCTGCGAATAGTGG
18S	Forward	CTACCACATCCAAGGAAGCA
	Reverse	TTTTTCGTCACTACCTCCCCG

Author Manuscript

Author Manuscript

Author Manuscript

Author Manuscript

**TABLE 3:**

Significantly changed lipids in fatostatin-treated HTM cells using lipidomic volcano analysis

Lipid names	FC	log2(FC)	raw. p-value	-LOG10(p)
LPS(O-18:0)	0.73346	-0.4472	0.013767	1.8612
LPS(17:2)	0.761	-0.39403	0.015029	1.8231
[TG(51:7),TG(50:0)]_FA16:0	0.79898	-0.32376	0.021917	1.6592
[TG(51:7),TG(50:0)]_FA18:0	0.84839	-0.23721	0.012095	1.9174
[TG(48:6)]_FA16:0	0.86119	-0.2156	0.0047502	2.3233
Cer(d18:1/25:0)	0.87544	-0.19191	0.0076135	2.1184
Cer(d18:1/26:0)	0.89366	-0.1622	0.038527	1.4142
PS(42:3)	0.89831	-0.15472	0.0070595	2.1512
[TG(55:7),TG(54:0)]_FA14:0	0.89844	-0.15451	0.0074426	2.1283
[TG(47:4)]_FA16:0	0.9026	-0.14784	0.04484	1.3483
DG(36:6)_C18:1	0.90803	-0.13919	0.019259	1.7154
[TG(48:3)]_FA18:1	0.9121	-0.13274	0.021998	1.6576
DG(36:3)_C18:0	0.91483	-0.12842	0.046872	1.3291
DG(37:6)_C18:1	0.91882	-0.12214	0.0205	1.6882
[TG(51:9),TG(50:2)]_FA18:3	0.92489	-0.11265	0.002672	2.5732
DG(44:8),DG(43:1)_C18:1	0.92699	-0.10938	0.014584	1.8361
PS(P-34:1)	0.92853	-0.10697	0.027975	1.5532
[TG(45:5)]_FA14:0	0.92923	-0.10589	0.026106	1.5833
[TG(50:3)]_FA14:0	0.93005	-0.10462	0.0077825	2.1089
DG(37:6)_C18:2	0.93198	-0.10164	0.01922	1.7162
[TG(49:3)]_FA18:3	0.93231	-0.10112	0.011167	1.9521
[TG(38:1)]_FA14:0	0.93565	-0.09596	0.038698	1.4123
DG(O-40:9),DG(38:2)_C18:1	0.93997	-0.08932	0.0032856	2.4834
DG(31:2),DG(P-14:0/18:1)_C18:2	0.94248	-0.08546	0.043189	1.3646
DG(38:3)_C18:2	0.94465	-0.08216	0.013449	1.8713
[TG(47:2)]_FA18:0	0.94859	-0.07614	0.011691	1.9322
[TG(49:5)]_FA18:2	0.94948	-0.07479	0.044194	1.3546
[TG(47:3)]_FA18:2	0.95833	-0.0614	0.01122	1.95
[TG(52:6)]_FA14:0	0.96963	-0.04449	0.015535	1.8087
[TG(54:5)]_FA18:3	0.97092	-0.04257	0.049176	1.3083
[TG(64:13),TG(63:6)]_FA18:1	1.0156	0.022367	0.015558	1.808
[TG(66:18),TG(65:11),TG(64:4)]_FA18:2	1.0165	0.023677	0.034418	1.4632
[TG(56:8),TG(55:1)]_FA18:3	1.0298	0.042352	0.00057611	3.2395
[TG(66:6)]_FA18:0	1.0303	0.043038	0.040248	1.3953
[TG(64:16),TG(63:9),TG(62:2)]_FA18:0	1.0313	0.044472	0.0087831	2.0564
[TG(62:8),TG(61:1)]_FA14:0	1.0352	0.049884	0.037112	1.4305
FA(31:0)	1.0369	0.052214	0.003511	2.4546

Lipid names	FC	log2(FC)	raw. p-value	-LOG10(p)
[TG(48:8),TG(47:1)]_FA18:2	1.037	0.052364	0.017224	1.7639
[TG(64:11),TG(63:4)]_FA18:3	1.0385	0.054432	0.029844	1.5251
[TG(52:10),TG(51:3)]_FA16:1	1.051	0.071799	0.039386	1.4047
[TG(42:2)]_FA18:2	1.0513	0.072178	0.016568	1.7807
FA(28:3)	1.0554	0.077799	0.023569	1.6277
SM(d18:1/25:0)	1.0571	0.080177	0.04653	1.3323
FA(26:2)	1.0578	0.081086	0.0062176	2.2064
[TG(64:11),TG(63:4)]_FA18:0	1.0604	0.084554	0.046904	1.3288
[TG(59:13),TG(58:6)]_FA16:0	1.0635	0.088755	0.026298	1.5801
[TG(43:2)]_FA18:1	1.0655	0.091595	0.020429	1.6897
[TG(45:2)]_FA14:0	1.0747	0.10394	0.034808	1.4583
[TG(56:7),TG(55:0)]_FA16:0	1.0757	0.10524	0.041985	1.3769
[TG(56:6)]_FA16:0	1.0804	0.1115	0.017136	1.7661
[TG(42:2)]_FA14:0	1.0824	0.11424	0.037315	1.4281
[TG(46:4)]_FA18:3	1.0921	0.12715	0.04208	1.3759
[TG(47:4)]_FA18:1	1.0943	0.12999	0.032941	1.4823
[TG(50:4)]_FA16:1	1.0964	0.13278	0.0081318	2.0898
FA(40:6)	1.0967	0.13317	0.011971	1.9219
[TG(54:5)]_FA16:0	1.1035	0.14209	0.032934	1.4824
FA(8:1)	1.1108	0.15154	0.022394	1.6499
[TG(41:0)]_FA18:0	1.1137	0.15534	0.0016727	2.7766
PC(36:3),PC(P-37:2)	1.1324	0.17942	0.041981	1.377
PE(42:4)	1.1434	0.19338	0.036597	1.4366
PE(30:0),PE(O-31:0)	1.1764	0.23443	0.023423	1.6304
DG(33:2)_C18:0	1.2035	0.2672	0.0017644	2.7534
PE(35:4),PE(O-36:4),PE(P-36:3)	1.2087	0.27346	0.0096295	2.0164
FA(14:1)	1.2135	0.27917	0.04429	1.3537
DG(33:4)_C18:2	1.2209	0.28789	0.0045654	2.3405
PC(31:2),PC(O-32:2),PC(P-32:1)	1.2282	0.29658	0.048578	1.3136
PE(36:7),PE(35:0),PE(O-36:0)	1.2336	0.30282	0.0094306	2.0255
PE(39:8),PE(O-40:8),PE(P-40:7),PE(38:1),PE(O-39:1),PE(P-39:0)	1.236	0.30568	0.032059	1.494
SM(d16:1/22:1)	1.2885	0.36569	0.0041656	2.3803
PC(34:3),PC(P-35:2)	1.3119	0.39163	0.023755	1.6242
PC(42:8),PC(41:1),PC(O-42:1),PC(P-42:0)	1.3475	0.43025	0.032877	1.4831
PC(37:6),PC(O-38:6),PC(P-38:5)	1.3497	0.4326	0.042341	1.3732
PC(42:7),PC(41:0),PC(O-42:0)	1.3736	0.45791	0.041498	1.382
PC(35:5),PC(O-36:5),PC(P-36:4)	1.5893	0.66842	0.0023312	2.6324
SM(d16:1/20:1)	1.6734	0.74278	0.0090041	2.0456
PC(30:3)	1.6764	0.74541	0.039106	1.4078

Lipid names	FC	log <sub>2</sub> (FC)	raw. p-value	-LOG <sub>10</sub> (p)
<b>PC(32:4)</b>	1.8924	0.92018	0.021488	1.6678
<b>Cer(d20:0/26:0)</b>	1.9283	0.94735	0.0084497	2.0732
<b>PC(32:3),PC(P-33:2)</b>	2.4561	1.2964	0.0031201	2.5058

Lipids significantly changed in fatostatin-treated compared to DMSO-treated HTM cells. Columns (left to right) show the lipid name, FC (fold change), log<sub>2</sub>(FC), raw p-value, and -log<sub>10</sub>(p) based on lipidomic volcano analysis, where n = 4 (biological replicates). A total of 79 specific lipids were above the threshold ( $|FC| > 1$  and  $p < 0.05$ ), log<sub>2</sub>(FC) < 0 indicates decreased lipids in fatostatin-treated HTM cells, whereas log<sub>2</sub>(FC) > 0 indicates increased lipids in fatostatin-treated HTM cells.

Author Manuscript

Author Manuscript

Author Manuscript

Author Manuscript



**TABLE 4:**

The most relevant pathways involved in fatostatin-treated HTM cells using lipidomic pathway analysis

Pathways	Total Compound	Hits	Raw p	FDR	Impact
Glycosylphosphatidylinositol (GPI)-anchor biosynthesis	14	1	0.17694	0.65345	0.00399
Glycerophospholipid metabolism	36	4	0.40972	0.65345	0.26332
Arachidonic acid metabolism	36	1	0.46277	0.65345	0
Linoleic acid metabolism	5	1	0.46277	0.65345	0
alpha-Linolenic acid metabolism	13	1	0.46277	0.65345	0
Biosynthesis of unsaturated fatty acids	36	1	0.49008	0.65345	0
Sphingolipid metabolism	21	2	0.83211	0.88546	0.26978
Steroid biosynthesis	42	1	0.88546	0.88546	0

The table shows the detailed results for pathways relevant to fatostatin treatment. Columns (left to right) denote the pathway names, the total number of compounds in the pathway (Total Compound), the matched number from the lipidomics data (Hits), the original p value calculated from the enrichment analysis (Raw p), the p-value adjusted using False Discovery Rate (FDR), and the pathway impact value calculated from pathway topology analysis (Impact).